



# Predicting the post-bifurcated patterns of architected materials using group-theoretic tools

Rachel Azulay, Christelle Combescure

## ► To cite this version:

Rachel Azulay, Christelle Combescure. Predicting the post-bifurcated patterns of architected materials using group-theoretic tools. *Journal of the Mechanics and Physics of Solids*, 2024, 187, pp.105631. 10.1016/j.jmps.2024.105631 . hal-04537593

**HAL Id: hal-04537593**

**<https://hal.science/hal-04537593>**

Submitted on 8 Apr 2024

**HAL** is a multi-disciplinary open access archive for the deposit and dissemination of scientific research documents, whether they are published or not. The documents may come from teaching and research institutions in France or abroad, or from public or private research centers.

L'archive ouverte pluridisciplinaire **HAL**, est destinée au dépôt et à la diffusion de documents scientifiques de niveau recherche, publiés ou non, émanant des établissements d'enseignement et de recherche français ou étrangers, des laboratoires publics ou privés.

# Predicting the Post-bifurcated Patterns of Architected Materials Using Group-Theoretic Tools

Rachel Azulay, Christelle Combescure

V2 : 14/02/2024

## Abstract

Extensive studies on hexagonal honeycombs under in-plane compression have demonstrated that the structure's symmetry plays a decisive part in the emergence of deformation patterns in post-bifurcated configurations. In this work, the aim is to take advantage of this property by presenting a new group-theoretic approach to list the various attainable post-bifurcated patterns of periodic architected materials.

As of today, some group-theoretic approaches have been elaborated for determining the post-bifurcated paths and thus patterns of a symmetric system submitted to specific loading conditions. However, the application of these approaches requires knowledge of the system's governing equations. By making use of another group-theoretic tool, this work predicts the various possible post-bifurcated configurations of a periodic architected material a priori of any non-linear computation by simply assessing the symmetry group of its undeformed configuration.

This approach is applied, as an example, to the buckling of regular hexagonal honeycombs but can be easily transferred to any periodic architected material. This work is a first step towards the elaboration of a more general process for the design of architected materials when harnessing post-bifurcated behaviour is essential.

## 1 Introduction

For the past 30 years, theoretical, numerical and experimental studies of regular hexagonal honeycombs under in-plane compression have been of particular interest. Indeed, the increasing challenges in material science for modern engineering applications have generated unprecedented enthusiasm in the study of a new class of materials, *architected materials* [1, 2], and for which 2D hexagonal structures have been a case study.

The pioneering studies that mechanically characterised the behaviour of a 2D regular hexagonal arrangement subject to in-plane compression were conducted by [3, 4, 5]. Through experiments and simulation, they observed the generation of three distinct patterns caused by buckling of the cell walls and involving multiple cells for given biaxiality ratios. Later on, other studies of honeycombs

attached to rigid substrates [6] and honeycombs where voids are filled with gels [7] were shown to exhibit new bifurcated patterns that had not yet been observed for the regular honeycomb composed of trusses and voids.

For design purposes, works on these materials then focused on theoretically and numerically determining the onset of buckling and the post-buckling behaviour of these structures. Indeed, studies on finding the onset of buckling for various load directions were carried out [8, 9] which coincided with previous experimental observations and showed that the patterns formed may occur at a larger wavelength than the primitive unit cell. An extensive review of the various methods for determining patterns stemming from instabilities in architected materials is presented in [10].

Of particular interest in this work is the study carried out by [11]. Indeed, their numerical investigation of the post-buckling response of hexagonal honeycombs was the first to establish the relationship between the initial symmetry of the structure and the symmetry in the patterns generated after the bifurcation point. As observed in previous experimental studies, a bifurcation phenomenon induces a loss of symmetry in the bifurcated path resulting in the change in shape and size of the representative periodic unit cell used to describe the pattern before and after the bifurcation point. Indeed, a periodic primitive unit cell composed of a single hexagon is enough to represent the geometry of the deformed configuration up to the bifurcation point, while a larger unit cell of  $2 \times 2$  hexagonal primitive cells seems to be necessary to capture the observable patterns after buckling. Such bifurcation is referred to as a *symmetry-breaking bifurcation*, as the symmetry of the bifurcated path is generically lower than the symmetry of the original structure. In the case of periodic architected materials such as hexagonal honeycombs, both point-group symmetries (referring to rotational, inversions and mirror symmetries) and translation symmetries can be broken when the patterns are formed.

The mechanisms of such pattern changes are subject to group-theoretic rules as thoroughly described by [12]. Two main tools are described in this book: (i) a symmetric treatment of the Lyapunov-Schmidt decomposition of the bifurcation equation near the bifurcation point and (ii) the Equivariant Branching Lemma which gives a result on the existence of bifurcated branches at the bifurcation point based on group theoretic considerations. The first tool was used for studying the flower-like mode in [13, 14] to solve the post-bifurcated branches. This method was further developed and used by [15, 16] for studying all three modes of various types of hexagonal honeycombs subject to in-plane compressive loads. Even if the group-theoretic Lyapunov-Schmidt decomposition has proven to be a very useful tool for determining the post-bifurcated behaviour of the structure, its application requires knowledge of the system's governing equations and needs to be performed for each boundary condition applied to the specimen. Taking a step back, the bifurcated path being directly linked to the symmetry of the structure, an appropriate group-theoretic tool should be able to predict at least some part of the post-bifurcated behaviour in architected materials *a priori* to any non-linear

computation. This is the role of the *Equivariant Branching Lemma* as first described by [17]. To the authors' knowledge, this method has only been used for simple point groups [14, 18, 19] and has never been applied neither for groups including some translation symmetries nor in this field of material science. However, the interested reader could start their journey into these types of methods by reading the following papers determining the various vibration modes of space grid and symmetric structures based on symmetry point groups arguments [20, 21] and then direct towards symmetry breaking bifurcation classifications with [22] and [23]. Additionally, most applications of the EBL stop at predicting the possible bifurcation subgroups [24] but nothing has been done to predict the bifurcated deformation patterns.

In this paper, a new group-theoretic-based method is presented. It makes use of the EBL to predict attainable post-bifurcated patterns of architected materials. Using the presented method, the paradigm is switched from a mechanical standpoint well suited for analysis to a mathematical standpoint more adapted for design purposes. Indeed, the first standpoint relies on a complex non-linear computational step that can be numerically costly, whereas the new proposed mathematical standpoint is based only on linear computations using the system symmetry and elastic strain energy only. Both the traditional and the newly proposed methods for predicting bifurcated deformation modes of architected materials are presented in Figure 1. In these schematics, gear symbols indicate design parameters that can be modified to attain different bifurcated patterns. As a consequence, a design step, represented by a black back-loop, would need to modify these design parameters to obtain suitable bifurcated patterns. The attentive reader would notice that the new proposed method separates the geometric design parameters from the material ones. This results in the generation of two short design loops as opposed to just one long loop in the conventional approach. Moreover, neither of these design loops depends on costly (represented by an hourglass symbol) non-linear computation in the newly suggested method, thereby expediting the entire design procedure. As such, the new design process is perfectly suited to be part of an optimisation process such as topology optimisation.

The layout of this paper is the following. Firstly, the appropriate group-theoretic background necessary to understand and apply the EBL in section 2 is presented. Then in section 3, the new proposed method for predicting the post-bifurcated deformation modes is detailed. This method is then applied to the regular hexagonal honeycomb subject to uniaxial and equibiaxial in-plane loads in section 4. Finally, a discussion and conclusion on this method and the presented results is proposed in section 5.

In the remaining of this paper, scalars, vectors and matrices will be respectively written with normal typesetting  $A$ , bold text  $\mathbf{B}$  and underlined bold text  $\underline{\mathbf{C}}$ .

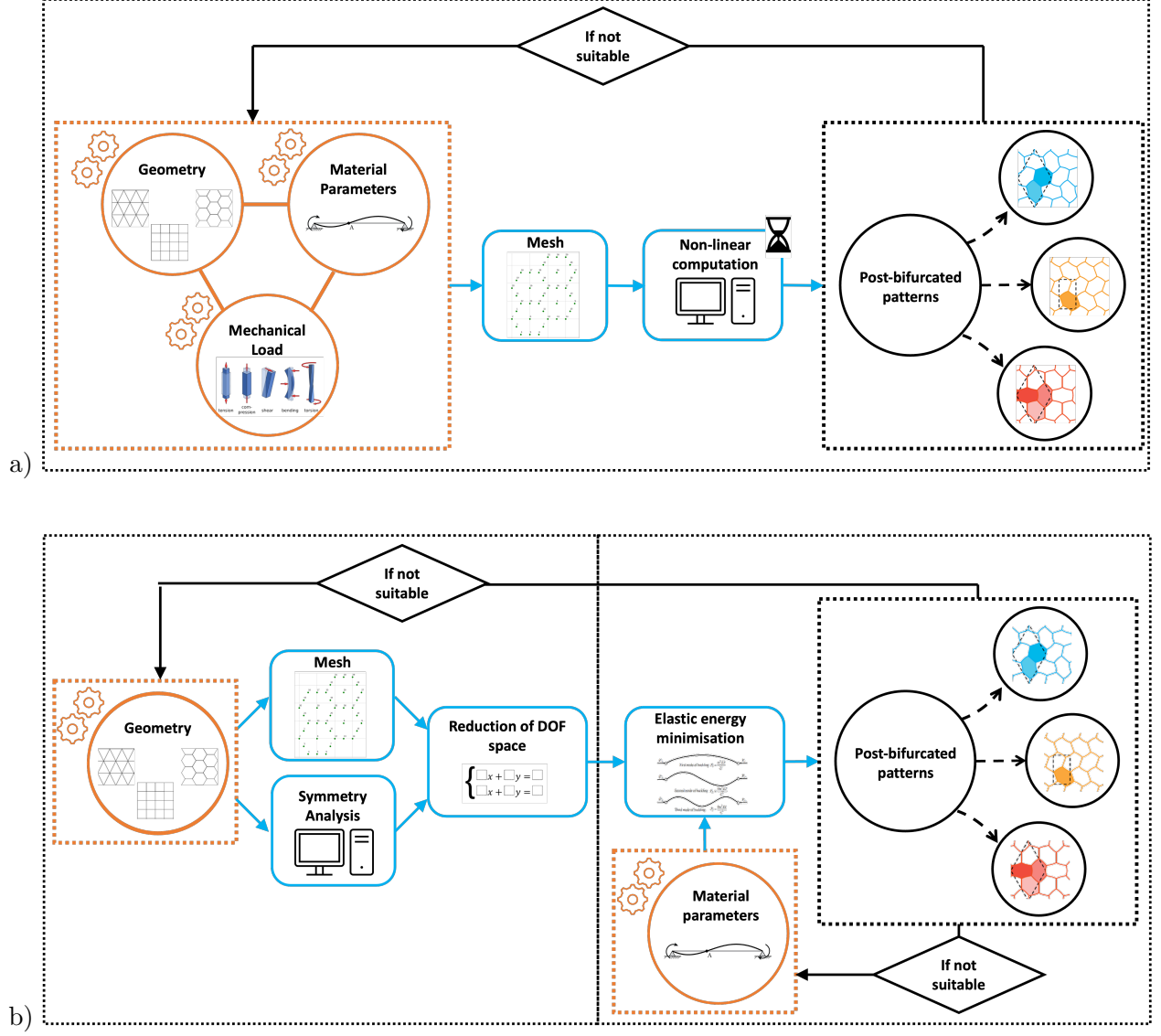


Figure 1: a) Traditional Mechanical based and b) New Mathematical based methods for predicting bifurcated deformation modes of architected materials. Gear symbols indicate design parameters that can be modified to attain different bifurcated patterns while an hourglass symbol emphasizes a computationally heavy step.

## 2 Group-theoretic preliminaries

As discussed in the introduction, the symmetry of an architected material strongly determines its post-bifurcated patterns. As a preliminary to the proposed method, this first section presents the group-theoretical background necessary for applying the tool that allows us to assess the post-bifurcated symmetry groups of the considered architected material: the Equivariant Branching Lemma.

## 2.1 Symmetry of the problem: Equivariance property

### 2.1.1 Problem setting

Let us consider a standard problem in mechanics: an elastic body  $\mathcal{B}$  in equilibrium occupying the region  $\Omega \in \mathbb{R}^3$  with surface area  $\Gamma$ . The current state of the body  $\mathcal{B}$  is represented by a state vector  $\mathbf{u} \in \mathbb{V}$ , where  $\mathbb{V}$  is the representation vector space (also called carrier space) of the problem. In the framework of finite element, the body is discretised into a finite number  $N$  of points so that its current state is described by the discrete displacement vector  $\mathbf{u} = (u_1, \dots, u_n)^T \in \mathbb{V} \equiv \mathbb{R}^N$ , where  $u_i$ ,  $i = 1..N$  is the degree of freedom vector of point  $i$ . **In this framework, the state vector is then the discrete displacement vector of the finite elements.**

If the mechanical system is conservative, the body's state can be described by a system of nonlinear equations that derive from its potential energy which is a twice differentiable function defined as:

$$\begin{aligned} \mathcal{E} : (\mathbb{V} \times \mathbb{R}) &\longrightarrow \mathbb{R} \\ (\mathbf{u}, \lambda) &\longmapsto \mathcal{E}(\mathbf{u}, \lambda) \end{aligned} \quad (1)$$

with  $\lambda \in \mathbb{R}$  the load parameter which acts as a multiplier of the problem's loading condition.

The behaviour of the mechanical problem is therefore governed by the nonlinear equilibrium equations:

$$\mathcal{E}_{,\mathbf{u}} \delta \mathbf{u} = 0, \quad \forall \delta \mathbf{u} \in \mathbb{V} \quad (2)$$

with  $\mathcal{E}_{,\mathbf{u}}$  the *Gateaux derivative* of the potential energy function.

Note that if the problem is not conservative, its behaviour is still described by a system of nonlinear equations that does not necessarily derive from a potential energy.

A solution of the nonlinear equilibrium equations is called an equilibrium solution. Equilibrium solutions depend on the load parameter  $\lambda$  and can be plotted on a graph as functions of that load parameter. All together, the equilibrium solutions for varying load parameters form a continuous line in that graph, called the equilibrium path. The particular equilibrium path that passes through the point in the graph of zero load parameter and null displacement vector is called the principal path and denoted as  $(\overset{0}{\mathbf{u}}(\lambda), \lambda)$ , often simplified as  $(\overset{0}{\mathbf{u}}, \lambda)$

### 2.1.2 Symmetry of the problem and equivariance

The symmetry of a problem **corresponds to the operations that leave the problem invariant**. All these operations are gathered in a set called a *symmetry group* and denoted  $G$  in this article. A group is a set of elements  $G = \{g_1, \dots, g_n\}$  together with an operation  $(*)$  that maps the set to itself. **In a mechanical system, the symmetry of a problem** is mathematically described by the *equivariance* of its governing equations (here the equilibrium equations 2) with respect to the symmetry group  $G$  of the system which is expressed as:

$$\mathbf{T}(g) \mathcal{E}_{,\mathbf{u}}(\mathbf{u}, \lambda) = \mathcal{E}_{,\mathbf{u}}(\mathbf{T}(g)\mathbf{u}, \lambda), \quad \forall g \in G, \forall \mathbf{u} \in \mathbb{V} \quad (3)$$

where  $g$  is an element of the group  $G$  and  $\underline{\mathbf{T}}(g)$  is a matrix representation of the action of this symmetry element on the vector space  $\mathbb{V}$ . For example, if one considers the action of a rotation  $r_\theta$  of angle  $\theta$  on the vector space  $\mathbb{V} = \mathbb{R}^2$ , then  $\underline{\mathbf{T}}(r_\theta)$  would simply be the well-know rotation matrix:

$$\underline{\mathbf{T}}(r_\theta) = \begin{bmatrix} \cos \theta & -\sin \theta \\ \sin \theta & \cos \theta \end{bmatrix}$$

The set of all matrices  $\{\underline{\mathbf{T}}(g)|g \in G\}$  form a faithful representation of the symmetry group  $G$  acting on the vector space  $\mathbb{V}$  meaning that distinct elements  $g$  of  $G$  are represented by distinct matrices  $\underline{\mathbf{T}}(g)$ . These matrices can generally be broken into smaller matrices called *irreducible representations* of the action of  $G$  and denoted  $\underline{\mathbf{T}}^\mu$ . These irreducible representations represent the action of group  $G$  on irreducible subspaces  $\mathbb{E}_\mu$ . The irreducible representations for finite groups are in a finite number and can be obtained through numerical procedures [25].

The equivariance property Equation 3 shows that transforming the governing equations is equivalent to writing them on the transformed vector. For instance, if  $r_\theta$ , the rotation by an angle  $\theta$ , is one of the system's symmetry, rotating the governing equations of the state vector  $\mathbf{u}$  by an angle  $\theta$  is equal to writing the governing equations for the rotated state vector  $\underline{\mathbf{T}}(r_\theta)\mathbf{u}$ .

On a side note, the equivariance property is established directly on the governing equations and, as a consequence, does not require the system to be conservative. When working with a conservative system, the equivariance property of the governing equations is a direct consequence of the invariance of the potential energy due to the symmetry group  $G$  which writes:  $\mathcal{E}(\underline{\mathbf{T}}(g)\mathbf{u}, \lambda) = \mathcal{E}(\mathbf{u}, \lambda)$ ,  $\forall g \in G$ ,  $\forall \mathbf{u} \in \mathbb{V}$ .

### 2.1.3 Critical points and stability operators

When following an equilibrium path by increasing the loading, critical points may arise that would lead to significant changes in the system's behaviour. A critical point on the principal equilibrium path is formally defined as an equilibrium state  $(\overset{0}{\mathbf{u}}_c, \lambda_c)$  where the stability operator becomes singular. Most of the time, this operator corresponds to the Jacobian matrix of the system. In this formalism, a critical point  $(\overset{0}{\mathbf{u}}_c, \lambda_c)$  arises when there exists at least one unit vector  $\overset{1}{\mathbf{u}} \in \mathbb{V}$  such that:

$$(\mathcal{E}_{,\mathbf{u}\mathbf{u}}(\overset{0}{\mathbf{u}}_c, \lambda_c) \overset{1}{\mathbf{u}}) \delta \mathbf{u} = 0, \quad \|\overset{1}{\mathbf{u}}\| = 1, \quad \forall \delta \mathbf{u} \in \mathbb{V} \quad (4)$$

Equation 4 merely states that a critical point is the state when at least one of the eigenvalues of the Jacobian matrix becomes null. The unit vectors  $\overset{1}{\mathbf{u}} \in \mathbb{V}$  of Equation 4 then correspond to the eigenvectors associated with the null eigenvalues of the Jacobian matrix. They are usually called *critical eigenvectors*. The set of all the critical eigenvectors  $\overset{1}{\mathbf{u}} \in \mathbb{V}$  spans the kernel space of the Jacobian matrix  $\mathcal{E}_{,\mathbf{u}\mathbf{u}}$ . Therefore, at a critical point, this kernel space has a dimension at least equal to 1. The kernel space of the Jacobian matrix is of interest because the bifurcated solutions exist in this space.

Critical points can be either limit points, where the solution to the non-linear governing equations remains unique or bifurcation points where this solution loses its uniqueness and a bifurcated path emerges from the critical point. **In the remainder of this article**, a distinction is made between pre and post-critical solutions by noting them  $\mathbf{u}^i$  and  $\mathbf{u}^{i+1}$ ,  $i \in \mathbb{N}$ , respectively.

The stability operator  $\mathcal{E}_{,\mathbf{u}\mathbf{u}}$  in the case of discretised mechanical systems corresponds to the tangent stiffness matrix. Differentiating the equivariance condition gives the commutation condition for the tangent stiffness matrix  $\mathcal{E}_{,\mathbf{u}\mathbf{u}}(\mathbf{u}, \lambda)$ :

$$\underline{\mathbf{T}}(g) \mathcal{E}_{,\mathbf{u}\mathbf{u}}(\mathbf{u}, \lambda) = \mathcal{E}_{,\mathbf{u}\mathbf{u}}(\mathbf{u}, \lambda) \underline{\mathbf{T}}(g), \quad \forall g \in G, \quad \forall \mathbf{u} \text{ equilibrium solution} \quad (5)$$

which can be written equivalently as:

$$\mathcal{E}_{,\mathbf{u}\mathbf{u}}(\mathbf{u}, \lambda) = \underline{\mathbf{T}}^{-1}(g) \mathcal{E}_{,\mathbf{u}\mathbf{u}}(\mathbf{u}, \lambda) \underline{\mathbf{T}}(g), \quad \forall g \in G, \quad \forall \mathbf{u} \text{ equilibrium solution} \quad (6)$$

This latter form of the commutation condition corresponds to a change of basis for the tangent stiffness matrix. **Essentially, the equivariance condition, implies that the kernel space can be determined by operating within a basis for the vector space  $\mathbb{V}$  that is distinct from the inherent basis arising from a finite element mesh. This basis, adapted to the symmetries of the system, will bring the stiffness matrix into a block-diagonal form. The matrices that bring about this block-diagonalisation are special representation matrices  $\underline{\mathbf{T}}$ . This is presented in detail in the coming section.**

## 2.2 Bifurcation and symmetry group of solutions

### 2.2.1 Symmetry group of the solutions

The symmetry group of an equilibrium solution  $\mathbf{u}$  is defined as **the set of operations that map this vector to itself. It is formally defined as the group  $G_{\mathbf{u}}$  such that**

$$G_{\mathbf{u}} = \{g \in G \mid \underline{\mathbf{T}}(g)\mathbf{u} = \mathbf{u}\} \quad (7)$$

where  $G$  is the symmetry group of the system.

**The attentive reader would then notice that the symmetry group of an equilibrium solution is a subgroup of the symmetry group of the system. This implies that it may possess a lower number of symmetry elements.**

**In the previous section two types of critical points were introduced: the bifurcation point where the solution loses its uniqueness and the limit point where it remains unique.** Generically, in the presence of a bifurcation point, a bifurcated solution  $\mathbf{u}^{i+1}$  will possess a lower symmetry than the pre-bifurcated solution  $\mathbf{u}^i$  whereas in the presence of a limit point, the post-critical solution has the same symmetry as the pre-critical one. The symmetries of a bifurcated solution form a subgroup of  $G$  called the *isotropy subgroup* of  $\mathbf{u}^{i+1} \in \mathbb{V}$ . By definition, an isotropy subgroup is the largest set of elements  $g \in G$  which leaves the displacement vector solution to the equilibrium equations invariant.



The symmetry group of equilibrium states on the principal path is then  $G_{\mathbf{u}} = G$ , while  $G_{\mathbf{u}_i} \subset G$ ,  $i \in \mathbb{N}^*$  is the symmetry group of any post-bifurcated solution. More generally speaking, at a symmetry-breaking bifurcation point one has  $G_{\mathbf{u}_{i+1}} \subset G_{\mathbf{u}_i}$ ,  $\forall i \in \mathbb{N}^*$ . **This can be rephrased as follows: some symmetries have been lost at the bifurcation point and thus, the symmetry group of the post-bifurcated solution is a subgroup of that of the pre-bifurcated solution.**

As stated in the previous section, at a bifurcation point  $(\mathbf{u}_c, \lambda_c)$ , the Jacobian matrix  $J(\mathbf{u}_c, \lambda_c)$  of the system becomes singular and the dimension of its kernel space is at least equal to 1. **It is possible to define the** symmetry group of the kernel space of the Jacobian matrix  $J_c(\mathbf{u}_c, \lambda_c)$  as:

$$G_{\ker(\mathcal{E}, \mathbf{u}\mathbf{u}(\mathbf{u}_c, \lambda_c))} = \{g \in G \mid \underline{\mathbf{T}}(g)\mathbf{u} = \mathbf{u}, \forall \mathbf{u} \in \ker(\mathcal{E}, \mathbf{u}\mathbf{u}(\mathbf{u}_c, \lambda_c))\} \quad (8)$$

Furthermore, the symmetry of the post-bifurcated solution  $\mathbf{u}^1$  is at least as high as the symmetry of the kernel space, **which leads to the following inclusions:**

$$G_{\ker(\mathcal{E}, \mathbf{u}\mathbf{u}(\mathbf{u}^1, \lambda))} \subseteq G_{\mathbf{u}^1} \subseteq G_{\mathbf{u}^0} = G \quad (9)$$

As a conclusion, it is possible to frame the symmetry group of the post-bifurcated solution in between the symmetry group of the system  $G$  and the symmetry group of the kernel space of the Jacobian matrix  $G_{\ker(\mathcal{E}, \mathbf{u}\mathbf{u}(\mathbf{u}^1, \lambda))}$ .

### 2.2.2 Isotypic decomposition and block diagonalisation

Now let us direct our attention to the various vector spaces in which it is possible to express our solutions. Recall from subsection 2.1.2 that the action of the group on a vector space is represented by representation matrices  $\underline{\mathbf{T}}$  and that it is possible to break these representation matrices into smaller matrices called irreducible representations of the action of  $G$  and denoted  $\underline{\mathbf{T}}^\mu$ . This decomposition formally writes as a direct sum:

$$\underline{\mathbf{T}} = \bigoplus_{\mu=1}^m m_\mu \underline{\mathbf{T}}^\mu \quad (10)$$

with  $m$  the number of irreducible representations of the symmetry group  $G$  and  $m_\mu$  is the multiplicity of the irreducible representation  $\underline{\mathbf{T}}^\mu$  in the decomposition. The blocks  $m_\mu \underline{\mathbf{T}}^\mu$  are called *isotypic components* of the representation  $\underline{\mathbf{T}}$ .

Each irreducible representation  $\underline{\mathbf{T}}^\mu$  represents the action of the group  $G$  on an irreducible subspace  $\mathbb{E}_\mu$ . As a consequence, the support of the isotypic component  $m_\mu \underline{\mathbf{T}}^\mu$  is a subspace  $\mathbb{V}_\mu$  of the full vector space  $\mathbb{V}$  called the isotypic subspace. This subspace decomposes itself as a direct sum of  $m_\mu$  times the same vector space  $\mathbb{E}_\mu$ :

$$\mathbb{V}_\mu = m_\mu \mathbb{E}_\mu = \underbrace{\mathbb{E}_\mu \oplus \dots \oplus \mathbb{E}_\mu}_{m_\mu \text{ terms}} \quad (11)$$

Since in Equation 10,  $\underline{\mathbf{T}}$  is a representation of the action of the group  $G$  on the full vector space  $\mathbb{V}$  and since the support of the isotypic component  $m_\mu \underline{\mathbf{T}}^\mu$  is the vector subspace  $\mathbb{V}_\mu$ , one thus have:

$$\mathbb{V} = \bigoplus_{\mu=1}^m \mathbb{V}_\mu = \bigoplus_{\mu=1}^m m_\mu \mathbb{E}_\mu \quad (12)$$

The decomposition on the left-hand side of Equation 12 is called the *isotypic decomposition* and is unique. On the contrary, the decomposition on the right-hand side is not unique since the choice of the subspace  $\mathbb{E}_\mu$ , which carries the irreducible representation  $\underline{\mathbf{T}}^\mu$ , is not unique.

Using the isotypic decomposition, a *symmetry-adapted basis* of vector space  $\mathbb{V}$  can be built [26]. Then, using the change of basis presented in Equation 6, the stability operator may be block-diagonalised, each block being associated with one of the subspaces  $\mathbb{V}_\mu$ :

$$\mathcal{E}_{,\mathbf{u}\mathbf{u}}(\mathbf{u}, \lambda) = \begin{bmatrix} \mathbb{V}_1 & & & \\ & \mathbb{V}_2 & & \\ & & \ddots & \\ & & & \mathbb{V}_m \end{bmatrix} \quad (13)$$

One special subspace  $\mathbb{V}_1$  corresponds to the trivial irreducible representation and solutions belonging to this subspace have the full symmetry  $G$  of the system. When the stability operator becomes singular, in its block-diagonalised form, it corresponds to only one block related to one isotypic subspace  $\mathbb{V}_\mu$  that becomes singular. If this block corresponds to the special subspace  $\mathbb{V}_1$ , the post-critical solution will have the same symmetry group as the pre-critical solution and the critical point is generically a limit point. On another hand, when a symmetry-breaking bifurcation point arises, the unstable block corresponds to any other subspace  $\mathbb{V}_\mu$ ,  $\mu \in \llbracket 2, m \rrbracket$ . Then, **since the subspace  $\mathbb{V}_\mu$  is support of  $m_\mu$ -times the irreducible representations  $\underline{\mathbf{T}}^\mu$** , the bifurcation point is said to be associated with the irreducible representation  $\underline{\mathbf{T}}^\mu$ . **To be more precise, it is only one sub-block, that corresponds to one of the  $G$ -irreducible subspace  $\mathbb{E}_\mu$ , that uniformly goes to 0 at the symmetry breaking bifurcation point. Consequently, the kernel space of the Jacobian matrix corresponds to that subspace  $\mathbb{E}_\mu$ . Therefore,** the symmetry of the kernel space of the Jacobian matrix  $G_{\ker(J_c(\mathbf{u}_c, \lambda_c))}$  coincides with the group  $G^\mu$ , called the kernel of the irreducible representation  $\underline{\mathbf{T}}^\mu$ , and defined as:

$$G^\mu = \{g \in G \mid \underline{\mathbf{T}}^\mu(g) = I_{n^\mu}\} \quad (14)$$

where  $I_{n^\mu}$  is the square identity matrix of dimension  $n^\mu$ ,  $n^\mu$  being the dimension of the  $G$ -irreducible subspace  $\mathbb{E}_\mu$ . **This kernel is nothing more than the set of all the operations of the irreducible representation that are represented by identity matrices. It is directly determined from group-theoretic considerations and does not require any prior knowledge of the Jacobian matrix.**

Finally, **using this information and putting it into the framing relation stated in Equation 9**, lower and upper bounds are obtained for the symmetry group of the bifurcated solution as follows:

$$G^\mu \subseteq G_{\mathbf{u}} \subseteq G \quad (15)$$

### 2.3 Predicting possible symmetry groups of the bifurcated solution: the Equivariant Branching Lemma

The question is now how to determine the symmetry group  $G_{\mathbf{u}}$  of the bifurcated solution  $\frac{1}{\mathbf{u}}$ . This is done using the *Equivariant Branching Lemma* (EBL) as stated by [17] which concludes on the existence and symmetry of a bifurcated solution.

The EBL makes use of the dimension of the fixed-point subspace of the isotropy subgroups  $G_{\mathbf{u}}$ . The fixed-point subspace of a subgroup  $H$  is defined as the set of vectors  $\mathbf{u} \in \mathbb{V}$  which are invariant under the actions of the group:

$$\text{Fix}_{\mathbb{V}}(H) = \{\mathbf{u} \in \mathbb{V} \mid \underline{\mathbf{T}}(g)\mathbf{u} = \mathbf{u}, \forall g \in H\} \quad (16)$$

Its dimension can be found using the trace formula:

$$\dim \text{Fix}_{\mathbb{V}}(H) = \frac{1}{|H|} \sum_{h \in H} \text{tr}(\underline{\mathbf{T}}(h)) \quad (17)$$

where  $\underline{\mathbf{T}}(h)$  is the matrix group representation of the action of group element  $h \in H$  on the vector space  $\mathbb{V}$ .

In Equation 17,  $\text{tr}(\underline{\mathbf{T}}(h))$  is the trace of the matrix group representation  $\underline{\mathbf{T}}(h)$  for the group element  $h$ . This is also known, in representation theory, as the *character* of this representation usually denoted  $\chi_{\mathbf{T}}(h)$ . **Characters of the most common finite group irreducible representations are tabulated in standard textbooks.**

The *Equivariant Branching Lemma* states:

Consider  $(\mathbf{u}_c, \lambda_c)$ , a symmetry breaking bifurcation point associated with the irreducible representation  $\underline{\mathbf{T}}^\mu$ . If  $H \subset G$  is an isotropy subgroup of  $G$  for  $\mathbf{u} \in \mathbb{E}_\mu$  satisfying  $\dim \text{Fix}_{\mathbb{E}_\mu}(H) = 1$ , then a bifurcating path with  $H$ -symmetry exists.

In other terms, bifurcation problems with symmetry group  $G$  generically exhibit solutions corresponding to isotropy subgroups with one-dimensional fixed-point subspaces.

By definition, an isotropy subgroup is the largest set of elements  $g \in G$  which leaves the displacement vector solution to the equilibrium equations invariant. As a consequence, an isotropy subgroup  $H$  is maximal [27], meaning that no subgroup  $K$  of  $G$  can be found so that  $H \subset K \subset G$ . The idea behind this lemma is that, since the symmetry group  $H = G^\mu$  is a lower bound for the symmetry group of the bifurcated solution  $G_{\mathbf{u}}$ , if  $G^\mu$  is maximal, then it has to be equal to  $G_{\mathbf{u}}$ . Otherwise, a supergroup  $K$  of  $G^\mu$  is maximal and is then equal to  $G_{\mathbf{u}}$ .

**In practice,** the list of all the isotropy subgroups with one-dimensional fixed-point subspaces gives the symmetry groups of the bifurcated solution of the problem satisfying the initial symmetry. Note that the given list is not exhaustive since the EBL gives a sufficient but not necessary condition for a bifurcating branch to emerge from the principal path.

### 3 Proposed group theoretic method

In this section, the new group theoretic method used for determining the post-bifurcated patterns of a periodic architected material is detailed. In the first step, the symmetry groups of the bifurcated solutions are determined using the EBL, and then the associated post-bifurcated patterns are identified. In this section, it is assumed that the symmetry group  $G$  of the system is finite.

#### 3.1 Symmetry analysis: determining symmetry groups of the bifurcated solutions

The determination of the symmetry groups of the bifurcated solutions is based on the EBL. The EBL states that the symmetry group of a bifurcated solution belonging to an irreducible subspace  $\mathbb{E}_\mu$  is an *isotropy subgroup* of the symmetry group of the problem with a one-dimensional fixed-point space. It is therefore necessary to first establish the decomposition of the representation space  $\mathbb{V}$  into irreducible subspaces  $\mathbb{E}_\mu$  in order to determine if the subspace  $\mathbb{E}_\mu$  appears in this decomposition. Once this decomposition is determined, the isotropy subgroups can be listed for each irreducible subspace  $\mathbb{E}_\mu$  appearing in the isotypic decomposition. Indeed, these isotropy subgroups are candidates for the symmetry groups of the solutions that satisfy the equilibrium equations [24]. In the last step, the dimension of the fixed-point space of these isotropy subgroups for the irreducible subspace  $\mathbb{E}_\mu$  can be computed in order to conclude on the existence of a bifurcated solution having this symmetry using the EBL.

The symmetry group of the problem  $G$  is supposed to be finite. As a consequence, it has a finite number of irreducible representations  $\underline{\mathbf{T}}^\mu$ ,  $\mu \in \llbracket 1, m \rrbracket$  and a finite number of associated irreducible subspaces  $\mathbb{E}_\mu$ . Since the EBL applies to fixed-point subspaces computed for the subspaces  $\mathbb{E}_\mu$  of the decomposition presented in Equation 12, this decomposition has to be determined. In the right-hand side of Equation 12, the subspace multiplicity  $m_\mu$  appears. This multiplicity can be computed using the following formula:

$$m_\mu = \frac{1}{|G|} \sum_{g \in G} \chi_{\mathbf{T}^\mu}(g) \chi_{\mathbf{T}}(g) \quad (18)$$

where it is reminded that  $\chi_{\mathbf{T}}(g)$  corresponds to the trace of the matrix representation  $\underline{\mathbf{T}}(g)$ .

If the multiplicity  $m_\mu$ , computed by Equation 18, appears to be null then the irreducible subspace  $\mathbb{E}_\mu$  does not appear in the decomposition **and will not be considered for the rest of the procedure**.

Once the decomposition **into irreducible subspaces** is determined, the EBL works on isotropy subgroups  $H$  of  $G$  for an irreducible subspace  $\mathbb{E}_\mu$ . The isotropy subgroups then have to be determined for each irreducible subspace  $\mathbb{E}_\mu$  appearing in the decomposition, except for the isotypic subspace  $\mathbb{V}_1$  related to the trivial irreducible representation and which corresponds to limit points preserving the symmetry of the system and not symmetry breaking bifurcation points. The determination of the isotropy subgroups for each irreducible subspace  $\mathbb{E}_\mu$  is done using the following algorithm:

---

**Algorithm 1** Computation of isotropy subgroups of group  $G$  of a given irreducible subspace  $\mathbb{E}_\mu$

---

**Input:** Subgroups of  $G$ , irreducible representation  $\underline{\mathbf{T}}^\mu$  associated with irreducible subspace  $\mathbb{E}_\mu$   
**for** each subgroup  $H \subset G$  **do**  
    **for** each subgroup  $K$  of  $G$  such that  $H \subset K \subset G$  **do**  
        **if**  $\dim \text{Fix}_{\mathbb{E}_\mu}(K) = \dim \text{Fix}_{\mathbb{E}_\mu}(H)$  **or**  $\dim \text{Fix}_{\mathbb{E}_\mu}(H) = 0$  **then**  
             $H$  is not an isotropy group for  $\mathbb{E}_\mu$   
        **end if**  
    **end for**  
**end for**  
**Output:** list of isotropy subgroups

---

This algorithm is based on two criteria:

1. for a subgroup to be an isotropy subgroup, the dimension of its fixed-point space cannot be equal to zero. Indeed, according to the definition of a fixed-point space given in Equation 16, if the dimension of this space is equal to zero then there is no vector  $\mathbf{u} \in \mathbb{E}_\mu$  that is invariant under the action of the group and thus no action of the group leaves a vector  $\mathbf{u} \in \mathbb{E}_\mu$  invariant and the isotropy subgroup would be empty ;
2. the definition of an isotropy subgroup is the largest set of elements  $g \in G$  which leaves the displacement vector  $\mathbf{u} \in \mathbb{E}_\mu$  invariant. As such, if  $K$  is an isotropy supergroup of  $H$  and the dimensions of the fixed-point spaces of both groups are equal,  $H$  cannot be an isotropy subgroup of  $G$  as  $\mathbf{u}$  is invariant by not only the elements of  $H$  but also those of  $K$ .

Authors point out that this algorithm is the same as the one proposed in [28].

The last step for applying the EBL is to check which isotropy subgroups have one-dimensional fixed-point space using the trace formula stated in Equation 17. The list computed via the previous algorithm is then reduced using the EBL: the isotropy subgroups whose fixed-point space dimension is not equal to one cannot be considered as possible post-bifurcated subgroups.

Therefore, at the end of this step, a list of the  $N$  possible post-bifurcated subgroups  $\{G_{\mathbf{u}}^1, \dots, G_{\mathbf{u}}^k\}$ ,  $k \in \mathbb{N}^*$  is obtained, for a problem with symmetry group  $G$ . In other terms, this first step provides a list of predicted post-bifurcated subgroups. Each of these subgroups contains a set of symmetry operations that would leave a post-bifurcated equilibrium solution invariant. If the subgroup has a high symmetry, i.e. it contains a large number of elements, then this subgroup may define uniquely, up to an amplification factor, the state vector  $\mathbf{u} \in \mathbb{V}$ . However, in most cases, an additional step is required to determine the post-bifurcation patterns.

## 3.2 Determining patterns knowing symmetry groups of bifurcated solutions

Having computed the list of possible post-bifurcated symmetry groups, the question is now to determine the corresponding post-bifurcated deformation patterns. The procedure described in this section first consists in reducing the number of unknowns in the displacement vector  $\mathbf{u} = (u_1, \dots, u_n)^T \in \mathbb{V}$  using the post-bifurcated symmetry groups found previously along with the knowledge of the associate isotypic subspace  $\mathbb{V}_\mu$  to which this vector should belong to. Indeed, the symmetry elements contained in the post-bifurcated symmetry groups will impose relationships between the independent degrees of freedom of the displacement vector  $\mathbf{u}$  thus leading to the definition of a reduced displacement vector. And that vector should be in the isotypic vector space  $\mathbb{V}_\mu$  corresponding to the irreducible representation associated with the bifurcation point of interest. Then an energy argument is used to uniquely determine the pattern.

### 3.2.1 Reduction of DOF space

The reduction of the Degrees of Freedom (DOF) space is carried on in two steps. First using the possible symmetry groups, a reduced vector defined by a reduced number of independent DOF is defined for each symmetry group. Then, knowing that a bifurcation point is associated with a given irreducible representation, the reduced vector is projected into the corresponding isotypic subspace. Thus ensuring that this vector might belong to the null space of the (undefined) non-linear stiffness matrix.

Let start with the definition of the reduced vector. For each post-bifurcated symmetry group predicted at the end of the former state, the symmetry operations of the groups impose relationships between the various degrees of freedom of the displacement vector. Indeed, the symmetry operations are the operations that leave the displacement vector invariant. The action of a symmetry operation  $g$  on the vector space  $\mathbb{V}$  of the displacement vector is represented by the matrix  $\underline{\mathbf{T}}(g)$ . As such, the relationships between the DOF of the displacement vector can be determined by solving the following system of linear equations:

$$\{\underline{\mathbf{T}}(g)\overset{1}{\mathbf{u}} = \overset{1}{\mathbf{u}}\} \quad \forall g \in G_{\mathbf{u}}^i, \quad i \in \llbracket 1, k \rrbracket \quad (19)$$

Solving Equation 19 results in a reduced number of degrees of freedom for the displacement vector  $\overset{1}{\mathbf{u}}$  that is symmetric under the action of the post-bifurcated subgroup  $G_{\mathbf{u}}^i$ . This actually corresponds to projecting the vector  $\overset{1}{\mathbf{u}}$  that was in the vector space  $\mathbb{V}$  into the fixed-point space  $\text{Fix}_{\mathbb{V}}(G_{\mathbf{u}}^i)$  of the post-bifurcated subgroup  $G_{\mathbf{u}}^i$  with respect to the vector space  $\mathbb{V}$ . Using only these independent degrees of freedom, a reduced displacement vector  $\overset{1}{\tilde{\mathbf{u}}}$  can be defined.

In order to be a possible post-bifurcated mode, the reduced displacement vector  $\overset{1}{\tilde{\mathbf{u}}}$ , which is defined on the full mesh vector space  $\mathbb{V}$  has to belong to the null space of the non-linear stiffness matrix. Without prior knowledge of the loading, the non-linear stiffness matrix cannot be defined. However, recall from

section 2.2.2 that when the stiffness matrix becomes singular, it corresponds to only one isotypic subspace  $\mathbb{V}_\mu$  that becomes singular. Therefore, the next step is to project the reduced displacement vector  $\hat{\mathbf{u}}$  from the full vector space  $\mathbb{V}$  to the unstable isotypic subspace  $\mathbb{V}_\mu$ . This projection is done using the projection operators, which are represented by matrices, into the symmetry adapted basis defined in [26]:

$$\mathbf{P}_\mu = \frac{1}{|G|} \sum_{g \in G} \chi_{\mathbf{T}^\mu}(g) \mathbf{T}(g) \quad (20)$$

These projection matrices are then used to project the reduced vector  $\hat{\mathbf{u}}$  into the appropriate vector space  $\mathbb{V}_\mu$  as follows:  $\hat{\mathbf{u}} = \mathbf{P}_\mu \hat{\mathbf{u}}$

All these operations can be carried out formally using symbolic computation tools.

In some rare cases, the projected reduced displacement vector only depends on one independent degree of freedom and the post-bifurcated pattern can then be uniquely defined from that information only. This would correspond to the case when the fixed-point space of the post-bifurcated subgroup  $G_{\hat{\mathbf{u}}}^i$  with respect to the vector space  $\mathbb{V}$  is the same as the fixed-point space of the same post-bifurcated subgroup but with respect to the vector subspace  $\mathbb{E}_\mu$ . In that case, the only degree of freedom serves as a mode amplitude parameter. In most cases, several independent degrees of freedom are involved which could lead to several patterns depending on the chosen linear combination of these degrees of freedom. Then, an additional step is necessary at this point to uniquely determine the post-bifurcated pattern. This is done using the total potential energy of the system.

### 3.2.2 Elastic energy minimisation

The total potential energy of the system is generically given by:

$$\mathcal{E} = \frac{1}{2} \int_{\mathcal{D}} \underline{\boldsymbol{\sigma}} : \underline{\boldsymbol{\varepsilon}} \, d\Omega - \left[ \int_{\mathcal{D}} \mathbf{f} \cdot \mathbf{u} \, d\Omega + \oint_{\partial\mathcal{D}} \mathbf{t} \cdot \mathbf{u} \, d\Gamma \right] \quad (21)$$

It is assumed that the system is free of body forces  $\mathbf{f} = \mathbf{0}$ . Moreover, in the periodic cell, the rightmost term of Equation 21 is cancelled out by the periodic boundary conditions:

$$\oint_{\partial\mathcal{D}} \mathbf{t} \cdot \mathbf{u} \, d\Gamma = 0 \quad (22)$$

Therefore, the total potential energy simply corresponds to the strain energy of the unit cell:

$$\mathcal{E} = \frac{1}{2} \int_{\mathcal{D}} \underline{\boldsymbol{\sigma}} : \underline{\boldsymbol{\varepsilon}} \, d\Omega \quad (23)$$

If one considers a finite element description of the problem. The strain energy corresponds to the sum of the energies for all the finite elements inside the cell which can be expressed in terms of the total stiffness matrix of the unit cell  $\underline{\mathbf{K}}$ :

$$\mathcal{E} = \frac{1}{2} \mathbf{u}^T \underline{\mathbf{K}} \mathbf{u} \quad (24)$$

From now on consider that some undetermined loading will bring the system to a bifurcation point associated with irreducible representation  $\mathbf{T}^\mu$ . At that bifurcation point, as explained in subsection 2.2.2, the total stiffness matrix of the unit cell  $\underline{\mathbf{K}}$  becomes singular and its kernel space corresponds to one of the irreducible subspaces  $\mathbb{E}_\mu$ . Then the post-bifurcated equilibrium solution is sought in the intersection between this irreducible subspace and the fixed-point space of one of the possible post-bifurcated symmetry groups associated with this irreducible representation. In fact, from the end of the previous state, the projected reduced displacement vector belongs to the isotypic space  $\mathbb{V}_\mu$  since the irreducible  $\mathbb{E}_\mu$  is unknown without non-linear computation. Then the following conjecture is assumed: the null space of the stiffness matrix, for some loading, corresponds to the vector subspace in the isotypic space  $V_\mu$ . This subspace also corresponds to the smallest eigenvalue of the elastic stiffness matrix  $\underline{\mathbf{K}}_e$ .

In practice, looking for an equilibrium solution comes back to minimizing the total energy. At the bifurcation point, the principal branch and all the possible bifurcated branches have the same energy which means that looking for a post-bifurcated energy comes back to looking for the minimum of the incremental energy from the bifurcation point on the bifurcated branch. In our case, using the previous conjecture, an equilibrium state on the bifurcated branch will belong to the previously described intersection between the fixed-point space of the post-bifurcated symmetry group and the kernel of the total stiffness matrix.

Consider an increment of displacement in this intersection  $\delta \hat{\mathbf{u}} \in \mathbb{E}_\mu \cap \text{Fix}_{\mathbb{V}}(G_{\mathbf{u}}^i)$  due to an increment of loading  $\delta \lambda$ . Then, the incremental energy computes as

$$\mathcal{E}_\delta = \frac{1}{2} (\delta \hat{\mathbf{u}})^T \left( \hat{\underline{\mathbf{K}}}_e + (\lambda_c + \delta \lambda) \hat{\underline{\mathbf{K}}}_g \right) (\delta \hat{\mathbf{u}}) \quad (25)$$

where  $\lambda_c$  is the critical buckling load and the hat sign stands for the projection of the stiffness matrices in the vector space of  $\delta \hat{\mathbf{u}}$ . In the former equation, the total stiffness matrix which is, in general, non-linear with respect to the equilibrium state, is decomposed as a sum of the elastic stiffness matrix  $\hat{\underline{\mathbf{K}}}_e$  and a non-linear geometric matrix  $\hat{\underline{\mathbf{K}}}_g$  depending linearly on the load. This hypothesis is also known as *linear buckling analysis* and is applicable to systems composed of structural elements such as beams, plates or shells.

Given that  $\delta \hat{\mathbf{u}} \in \mathbb{E}_\mu$ , it is in the kernel of the non-linear stiffness matrix at the bifurcation point:  $\hat{\underline{\mathbf{K}}} \delta \hat{\mathbf{u}} = \mathbf{0} \Leftrightarrow (\hat{\underline{\mathbf{K}}}_e + \lambda_c \hat{\underline{\mathbf{K}}}_g) \delta \hat{\mathbf{u}} = \mathbf{0}$ . Consequently, the incremental energy can be reduced to

$$\mathcal{E}_\delta = \frac{1}{2} \delta \lambda \delta \hat{\mathbf{u}} \hat{\underline{\mathbf{K}}}_g \delta \hat{\mathbf{u}} = \frac{-\delta \lambda}{2 \lambda_c} \delta \hat{\mathbf{u}} \hat{\underline{\mathbf{K}}}_e \delta \hat{\mathbf{u}} \quad (26)$$

Finally, the increment of displacement  $\delta \hat{\mathbf{u}}$  on the post-bifurcated branch has to be an equilibrium solution for the incremental energy  $\hat{\mathcal{E}}_\delta$ , meaning that it must minimise this energy. This corresponds to finding the smallest eigenvalue of the elastic stiffness matrix in the reduced space  $\hat{\underline{\mathbf{K}}}_e$ .



The energy minimisation uses the fact that the energy can then be re-written in terms of eigenvectors  $\hat{\boldsymbol{\eta}}_I$  and eigenvalues  $\alpha_I$  of the reduced elastic stiffness matrix  $\hat{\mathbf{K}}_e$ . Indeed, the increment of displacement  $\delta\hat{\mathbf{u}}$  on the post-bifurcated branch can be projected into the eigenspace of the elastic stiffness matrix as follows:  $\delta\hat{\mathbf{u}} = \sum_I b_I \hat{\boldsymbol{\eta}}_I$  which induces:

$$\hat{\mathcal{E}}_\delta = \frac{1}{2} \sum_I b_I^2 \hat{\boldsymbol{\eta}}_I^T \hat{\mathbf{K}}_e \hat{\boldsymbol{\eta}}_I = \sum_I b_I^2 \frac{1}{2} \alpha_I \hat{\boldsymbol{\eta}}_I^T \hat{\boldsymbol{\eta}}_I = \sum_I b_I^2 \frac{\alpha_I}{2} \quad (27)$$

under the assumption of normalized eigenvectors  $\hat{\boldsymbol{\eta}}_I$ .

Therefore the increment of displacement that minimises the energy from the bifurcation point corresponds to the eigenvector  $\hat{\boldsymbol{\eta}}_0$  associated with the smallest eigenvalue  $\alpha_0$  of  $\hat{\mathbf{K}}_e$ .

The computation of the smallest eigenvalue of the elastic stiffness matrix, reduced to the fixed-point space of  $G_{\mathbf{u}}^i$ , cannot be realized analytically and requires numerical computation. Additionally, this requires information on the material parameters that constitute the geometry of the architected material. At this stage only, the material parameters are inputted into the method.

The framework in which this method is proposed to be applied below uses beam elements which are suitable for linear buckling hypothesis. The method could use plate and shell elements as well. It is less clear if such an argument would hold in the case of solid 2D or 3D elements composed of soft materials, for instance.

As a summary, in the newly proposed method, the possible post-bifurcated deformation modes are predicted by an eigenvalue analysis of the reduced elastic stiffness matrix  $\hat{\mathbf{K}}_e$  conducted for each possible symmetry groups of bifurcated solutions.  $G_{\mathbf{u}}^i$ . This eigenvalue analysis provides, in a unique way, the post-bifurcated deformation patterns (or modes) that could emerge from a bifurcation point.

### 3.3 Summary of the method

Figure 1 b) presents a graphic summary of the newly proposed method for determining the post-bifurcated patterns of architected materials. In this schematic, the gear symbols indicate design parameters that can be modified to attain different bifurcated patterns. It appears obvious that the new proposed method separates the geometric design parameters from the material ones. Indeed, up to the reduction of the DOF space, the only information necessary for the computation is the specification of the geometry of the architected material periodic cell and the computations can be done analytically. The material parameters are only inputted for the elastic energy minimisation step. This creates two separate design loops that are available to the designer or an optimisation process. These two steps are represented by two dashed boxes on the Figure 1 b). Moreover, the method does not perform any non-linear computation. As such, it is fast and perfectly suited for design applications as part of a topology optimisation process, for instance.

Finally, the mechanical load design parameter is removed from the proposed method. This prevents

the load from selecting a given post-bifurcated pattern and allows our method to predict all the post-bifurcated patterns that could appear for a given architected material. It is then left to the designer or to an optimisation algorithm, in a final step, to find the appropriate loading that will select one or another target pattern.

## 4 Application on the regular hexagonal honeycomb

The new method presented in the previous section is now applied to the regular hexagonal honeycomb structure. This example has been chosen because, as presented in the introduction, it is a well-studied example that will allow us to validate the method and also to show its interest since the proposed method will predict new possible bifurcated patterns. Two loading conditions will be considered for this application: an equibiaxial loading and a uniaxial or biaxial loading. These loadings will be taken into account by only considering their symmetry groups and their intersection with that of the initial geometry of the honeycomb.

### 4.1 Symmetry analysis of the initial geometry

The infinite honeycomb can be described by a tessellation in the plane of the regular hexagon. The regular hexagon has symmetry group  $D_6$ . This symmetry group possesses 12 symmetry elements and can be generated by a rotation of order 6 (i.e. by the angle  $\frac{2\pi}{6}$ ), noted  $r_6$  around the out-of-plane axis passing through the centre of the hexagon and a mirror symmetry  $s$  with respect to a vertical plane passing through that same centre. From these two generators, the whole set of 12 symmetry elements of the symmetry group  $D_6$  can be constructed using the Cayley table of this group. **The chosen notation for the name of the group follows the classical notation from crystallography [26]. It uses the letter  $D$  when a mirror symmetry is one of the group elements (letter  $C$  would be used otherwise) and the number 6 to indicate the rotational order of the rotational generator element  $r_6$ . This group is also named  $C_{6v}$  in the Schoenflies notation.** Such a group which contains only point-wise operations is called a point-group.

As presented in the introduction, it has been shown in the literature that the post-bifurcated patterns require more than one hexagonal tile, also called primitive cell, to be captured [3, 4, 5, 15]. Indeed, at least  $2 \times 2$  primitive cells are necessary to show the diversity of the modes observed experimentally (see Figure 2). Consequently, it is chosen to work with the symmetry group:  $D_6 \ltimes (Z_2 \times Z_2)$  for the regular hexagonal honeycomb. In this notation, a semi-direct product  $\ltimes$  is used to combine the point group  $D_6$  of the regular hexagon with the cyclic group  $(Z_2 \times Z_2)$ . The reader is directed to standard mathematical textbooks for the definition of the semi-direct product [29]. The cyclic group  $(Z_2 \times Z_2)$  represents the inner translation symmetries along with the  $2 \times 2$  periodicity of the chosen unit cell. **This unit cell is presented on the right-hand side of Figure 2.** It is periodic along the periodicity vectors  $\alpha_1$  and  $\alpha_2$  and composed of **4 primitive cells: 2 primitive cells along the first lattice vector  $p_1$  and 2 primitive cells along the second lattice vector  $p_2$ .** As a consequence, it has inner translation

symmetries that allow it to go from one primitive cell to another along both lattice vectors  $p_1$  and  $p_2$  and along the vector built from the sum of these two vectors. After two such translations in each direction, the unit cell has been brought back to itself by periodicity. This means that the symmetry group of the inner translations of this unit cell is  $(Z_2 \times Z_2)$ , a group composed of 4 elements  $\{e, p_1, p_2, p_1 * p_2\}$ , where  $e$  represents the identity element. The generators of this group are noted  $p_1$  and  $p_2$  and represented Figure 2. These generators correspond to the periodicity vectors of the primitive cell. The symmetry group  $(Z_2 \times Z_2)$  has 4 symmetry elements and, as such, combined with point group  $D_6$  of 12 elements, the resulting symmetry group:  $D_6 \times (Z_2 \times Z_2)$  is composed of 48 elements and generated by four symmetry elements chosen to be  $r_6$ ,  $s$ ,  $p_1$  and  $p_2$ .

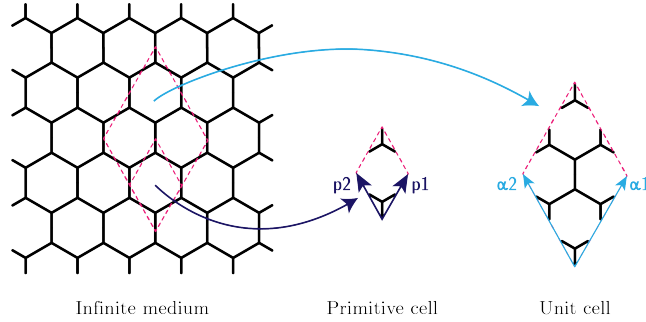


Figure 2: Difference between primitive and unit cells when considering the bifurcation of an infinite 2D honeycomb medium.

The reader's attention is drawn to the fact that a modelling choice has to be made at that point on the size of the unit cell leading to the cyclic group  $(Z_2 \times Z_2)$ . Indeed, contrary to other studies [15, 30] that make use of specific analysis known as Bloch-wave analysis to determine that size during the non-linear computation, the proposed method does not have such a tool implemented. This is a limitation of the method but authors believe that its numerical efficiency will make it possible to overcome that limitation by scanning rapidly using for instance parallelisation methods for the various unit-cell sizes.

Finally, the irreducible representations for the symmetry group  $D_6 \times (Z_2 \times Z_2)$  have to be determined. The irreducible representations for finite groups are in a finite number and can be obtained through numerical procedures [25]. In the present case, they have been obtained using the Groups, Algorithms, Programming (GAP) software [31]. Symmetry group  $D_6 \times (Z_2 \times Z_2)$  has 10 irreducible representations: 4 one-dimensional denominated with symbols  $A_1, A_2, B_1, B_2$  and 2 two-dimensional, named  $E_1$  and  $E_2$ . Together, all these 6 irreducible representations are identical to the irreducible representations of the point group  $D_6$ . The 4 additional three-dimensional irreducible representations, named  $T_1, T_2, T_3$  and  $T_4$ , are due to the semi-direct product with the translation group. GAP also tells us that group  $D_6 \times (Z_2 \times Z_2)$  can be decomposed into 33 subgroups classes. Inside a subgroup class, groups are related by conjugacy relations, meaning that they only differ by the orientation of their generator elements.

They are, in a sense, the same groups but expressed in a different basis. As a consequence, the subsequent analysis will be conducted in terms of symmetry classes more than in terms of symmetry groups. In order to help the reader understand the meaning of the various groups belonging to the same symmetry class, the symmetry patterns for the three groups of the symmetry class  $D_2 \times (Z_2 \times Z_2)$  are presented in Table 4 on the line corresponding to the irreducible representation  $E_1$ .

## 4.2 Modeling

The unit cell is modelled using standard Euler-Bernoulli beam finite elements, the parameters of which are summarized in Table 1.

Beam parameters		
$L$	0.5 cm	Strut length
$h$	0.05 cm	Strut thickness
$b$	1 cm	Strut depth
$S$	$0.05 \text{ cm}^2$	Strut cross-sectional area
$I$	$1.041667 \times 10^{-5} \text{ cm}^4$	Strut moment of inertia
$E$	69MPa	Material's Young modulus

Table 1: Table summarising the beam parameters

Employing linear interpolation for the axial displacement and cubic interpolation for the transverse displacement, the conventional shape functions from finite element beam theory are applied. These shape functions link the beam's end nodal displacements  $u_i, v_i$  and rotations  $\theta_i$  (referred to as degrees of freedom or DOFs) with the displacement of any point and rotation of the cross-section located inside the beam  $u(x), v(x), \theta(x)$ . The three DOFs for each node are gathered into the displacement vector  $\mathbf{u} = [u_1, v_1, \theta_1, \dots, u_N, v_N, \theta_N]$ , where  $N$  is the number of finite elements nodes in the mesh. As a consequence, the representation vector space of consideration is thus  $\mathbb{V} = \mathbb{R}^{3N}$ .

The mesh used to apply the method is presented in Figure 3. A mesh convergence study has been performed and the selected mesh provides converged results in terms of predicted bifurcated deformation patterns. The isolated points at the centre of each hexagon are only reference points introduced to track the inner translations and are not attached to any matter. As a consequence, they do not correspond to any finite element node.

The mesh and the choice of the Euler-Bernoulli beam element modelling impose a representation vector space. Given this representation vector space, the action of the symmetry group on this representation space has to be defined. It consists of defining the representation matrices  $\underline{\mathbf{T}}(g)$  for each symmetry element  $g$  in the symmetry group of the initial geometry  $D_6 \times (Z_2 \times Z_2)$ . Since all the 48 elements of this symmetry group are generated by only four elements, it is enough to define the representation matrices  $\underline{\mathbf{T}}(g)$  only for the four chosen generators  $r_6, s, p_1$  and  $p_2$ . The representation

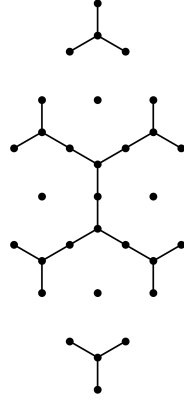


Figure 3: Mesh of the honeycomb unit cell. The isolated points at the centre of each hexagon are only reference points introduced to track the inner translations and are not attached to any matter. As a consequence, they do not correspond to any finite element node.

matrices carry information on both node permutations under the action of the symmetry element on the mesh and changes in displacement directions after applying a group action to the three degrees of freedom of a node. In particular, the group actions are first applied to the nodes of the unit cell and a nodal permutation matrix  $\underline{\mathbf{P}}(g)$  is generated by checking the finite element nodes which coincide with each other before and after the group action. This nodal permutation matrix is then combined with a  $3 \times 3$  matrix describing how the nodal degrees of freedom are affected by the group actions. As an example, the action of the rotational group generator  $r_6$  on the mesh is presented in Figure 4 where the rotated unit cell is surrounded by purple lines while the initial unit cell, reproduced by periodicity is represented delimited by grey lines. The purple-to-grey identification leads to the nodal permutation matrix  $\underline{\mathbf{P}}(r_6)$ . The cyan arrows represent the degrees of freedom of each node modified by the action of the group generator  $r_6$ . These rotated degrees of freedom can be deduced from the initial ones using the following  $3 \times 3$  matrix:

$$\underline{\mathbf{t}}(r_6) = \begin{bmatrix} \cos(\frac{\pi}{3}) & -\sin(\frac{\pi}{3}) & 0 \\ \sin(\frac{\pi}{3}) & \cos(\frac{\pi}{3}) & 0 \\ 0 & 0 & 1 \end{bmatrix} = \begin{bmatrix} \frac{1}{2} & -\frac{\sqrt{3}}{2} & 0 \\ \frac{\sqrt{3}}{2} & \frac{1}{2} & 0 \\ 0 & 0 & 1 \end{bmatrix} \quad (28)$$

### 4.3 Equibiaxial loading

The symmetry group of the problem is the intersection between the symmetry group of the architected material and the symmetry group of its loading conditions. For equibiaxial loading, the boundary condition's symmetry group is very symmetric since the macroscopic loading is isotropic. As a consequence, the boundary conditions are  $O(2)$ -symmetric. Therefore the symmetry group of the problem is  $D_6 \ltimes (Z_2 \times Z_2) \cap O(2) = D_6 \ltimes (Z_2 \times Z_2)$  (see Figure 5).

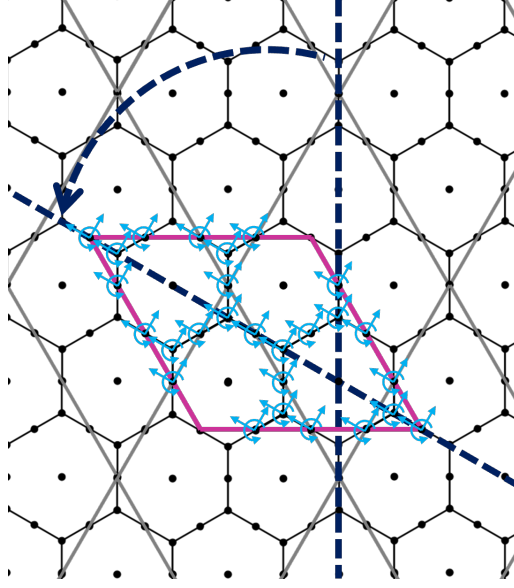


Figure 4: Example of the action of rotational group generator  $r_6$  on the finite element mesh and degrees of freedom. The rotated unit cell is surrounded by purple lines while the initial unit cell, reproduced by periodicity is represented surrounded by grey lines. The cyan arrows represent the degrees of freedom of each node modified by the action of the group generator  $r_6$

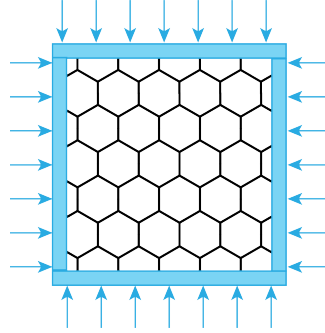


Figure 5: Schematic representation of a biaxial macroscopic load ( $O(2)$  symmetry) on the honeycomb lattice.

As stated in the symmetry analysis section along with the group-theoretic preliminaries,  $D_6 \ltimes (Z_2 \times Z_2)$  has 10 irreducible representations, but only one subspace  $\mathbb{E}_\mu$  associated with one irreducible representation will contain the singularity of the stability operator on the principal equilibrium path. The computation of the isotypic decomposition Equation 12 states that all of the isotypic subspaces appear in the decomposition. The Equivariant Branching Lemma will thus be applied to all of these subspaces since bifurcation is susceptible to happen in any of them.

Out of the 33 possible subgroup classes, only 23 are isotropy subgroup classes (counting the ini-

tial group) among which only 17 have one-dimensional fixed-point subspaces. These possible post-bifurcated subgroup classes for each irreducible representation are presented in Table 3. They are named using the name of one of the groups in the class. The superscripts  $s$  or  $h$  are used to identify whether the mirror symmetry generator corresponds to a vertical or a horizontal mirror whereas superscripts  $g$ ,  $g2$  and  $g3$  indicate various types of glide generators combining a mirror symmetry element with a translation. The number of groups in the class is given in parenthesis and the generators of the representative group are indicated in braces. In order to help the reader understanding the signification of the various names for the groups present in Table 3, a table presenting these names along with various shapes illustrating the symmetry groups is proposed Table 2. Indeed, the symmetry groups presented correspond to symmetry groups of well-known polygons except for symmetry group  $C_6$ , which corresponds to the symmetry of a hexagon that would have lost its mirror symmetries. The proposed shape for this group could be called a chiral hexagon. Moreover, note that the two groups  $D_3^s$  and  $D_3^h$  are both groups of an equilateral triangle but that triangle is standing up in the first case and rotated in the second, meaning that the mirror symmetry of  $D_3^s$  is vertical, whereas it is horizontal for  $D_3^h$ . The same happens for groups  $D_1^s$  and  $D_1^h$ . These shapes will be used at several places in the remaining of this article as a visual reminder of the meaning of the group theoretic names.







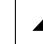
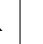
$D_6$	$C_6$	$D_3^s$	$D_3^h$	$D_2$	$C_2$	$D_1^s$	$D_1^h$
							

Table 2: Table presenting shapes illustrating the signification of the names for the symmetry groups used later in the chapter.

At this point, results presented in Table 3 are difficult to interpret. However, one can still extract information from this table based on understanding of its group-theoretic content. For instance, if a subgroup class includes the translations  $p_1$  and  $p_2$  as generators (or equivalently if their subgroup class name is composed with a semi-direct product with the group  $Z_2 \times Z_2$ ), then all four primitive cells inside the  $2 \times 2$  cell will deform in a similar manner. This is the case for the first six irreducible representations inherited from the point group  $D_6$  and located above the dashed line in Table 3. For the remaining four irreducible representations, the deformed pattern will be expected to have all four cells deformed in a different manner, except when a one of the translation remains in the generator (or equivalently when a semi-direct product with  $Z_2$  is present in the name of the subgroup class. Moreover, if a class has the symmetry element  $s$  as a generator, then the deformation pattern presents a vertical mirror symmetry. The integer  $n$  associated with the symmetry element  $c_n$  represents the order of the generating rotation. For example, a  $r_6$  symmetry is a rotation by an angle of  $\frac{2\pi}{6}$  whereas a  $r_3$  symmetry is a rotation by an angle of  $\frac{2\pi}{3}$ . Further comments can be made on the number of subgroup classes, i.e. the number of possible patterns, available for a given irreducible representa-



















Irreducible representation	Possible post-bifurcated subgroup classes (nb groups in class) {generators}
$A_1$	$D_6 \ltimes (Z_2 \times Z_2)$ (1) $\{p_1, p_2, r_6, s\}$ 
$A_2$	$C_6 \ltimes (Z_2 \times Z_2)$ (1) $\{p_1, p_2, r_6\}$ 
$B_1$	$D_3^s \ltimes (Z_2 \times Z_2)$ (1) $\{p_1, p_2, r_3, s\}$ 
$B_2$	$D_3^h \ltimes (Z_2 \times Z_2)$ (1) $\{p_1, p_2, r_3, h\}$ 
$E_1$	$D_2 \ltimes (Z_2 \times Z_2)$ (3) $\{p_1, p_2, r_2, s\}$ 
$E_2$	$D_1^h \ltimes (Z_2 \times Z_2)$ (3) $\{p_1, p_2, h\}$    $D_1^s \ltimes (Z_2 \times Z_2)$ (3) $\{p_1, p_2, s\}$ 
$T_1$	$D_6$ (4) $\{r_6, s\}$    $D_2 \ltimes Z_2$ (3) $\{p_2, r_2, s\}$ 
$T_2$	$D_2^g \ltimes Z_2$ (3) $\{sp_1, p_2, r_2\}$    $D_2$ (6) $\{r_2, s\}$    $C_6$ (4) $\{r_6\}$ 
$T_3$	$D_2^{g2} \ltimes Z_2$ (3) $\{r_2 p_1, p_2, s\}$    $D_3^s$ (4) $\{r_3, s\}$    $D_2^{g2}$ (6) $\{r_2 p_2, s\}$ 
$T_4$	$D_2^{g3} \ltimes Z_2$ (3) $\{sp_1, r_2 p_1, p_2\}$    $D_3^h$ (4) $\{r_3, h\}$    $D_2^{g2}$ (6) $\{r_2 p_2, s\}$ 

Table 3: Table of isotropy subgroup classes for each irreducible representation of  $D_6 \ltimes (Z_2 \times Z_2)$ . A dashed line separates irreducible representations inherited from the point group  $D_6$  from the ones that are due to the semi-direct product with the translation group

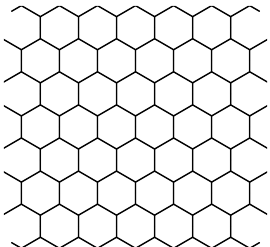

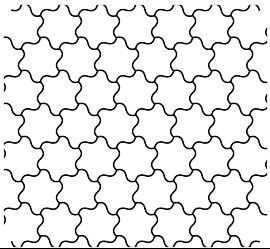

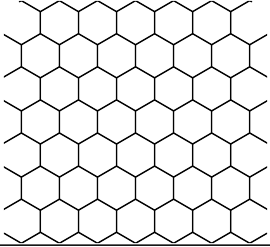

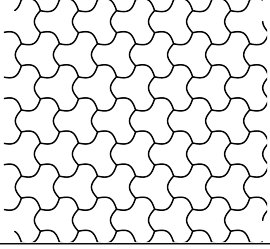

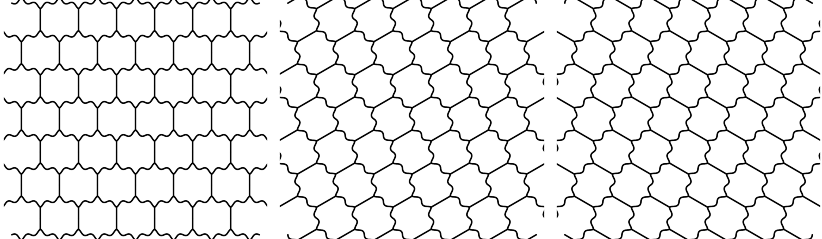

tion. The first five irreducible representations provide only one available deformation pattern, while the irreducible representations  $E_2$  and  $T_1$  provide two patterns each and the last three irreducible representations generate three patterns each.

Among these isotropy subgroup classes, three are of particular interest to us since they have already been reported in the literature. Indeed, [16] computed, from a non-linear finite element simulation, the post-bifurcated patterns of a hexagonal honeycomb subjected to equibiaxial loading. They provided the symmetry elements of their three computed post-bifurcated patterns for the regular honeycomb with circular cells under equibiaxial loading. By comparing the symmetry elements of these non-linearly predicted post-bifurcated patterns and the symmetry elements of the various predicted possible symmetry groups, it is possible to conclude that these predicted post-bifurcated groups are also found in the list of isotropy subgroup class of Table 3 for irreducible representation  $T_2$ : Mode I (also called alternating band mode) is group  $D_2^g \ltimes Z_2$ , Mode II (butterfly mode) corresponds to group  $D_2$  and finally Mode III (flower mode) is group  $C_6$ . It is then possible to quantitatively confirm that both the post-bifurcated groups of the patterns from the literature, stemming from a non-linear finite element simulation, and from the new proposed method are exactly the same even though the processes for obtaining them are completely different since the present study is conducted without any non-linear buckling analysis.

The second step of the method allows us to determine the possible post-bifurcated patterns of the



regular hexagonal honeycomb subjected to equibiaxial loading. These patterns are presented in Table 4. In order to help the reader understand the meaning of the various groups belonging to the same symmetry class, the three symmetry groups belonging to the same symmetry class  $D_2 \times (Z_2 \times Z_2)$  are presented for the irreducible representation  $E_1$  whereas only one group representative per class has been chosen for the other irreducible representations.

Irreducible Representation	Post-bifurcated patterns for each irreducible representation		
$A_1$			
$A_2$			
$B_1$			
$B_2$			
$E_1$ the 3 symmetry groups of the same class			

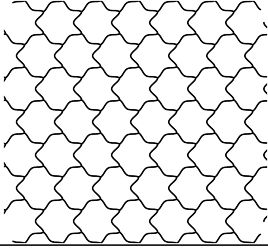
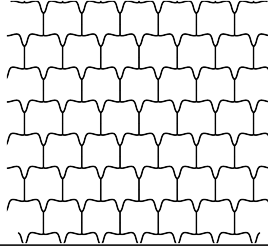

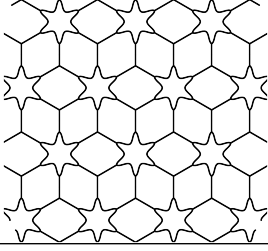
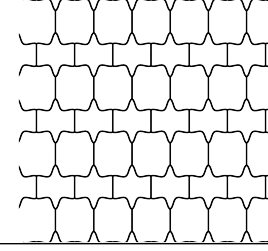

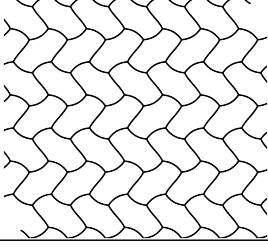
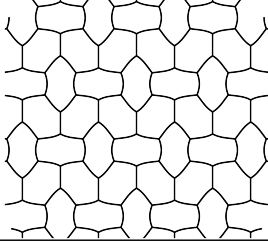
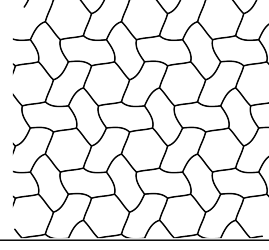
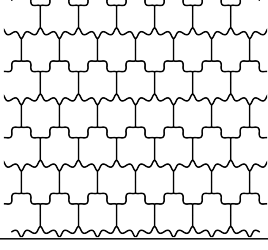
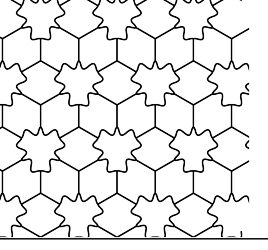
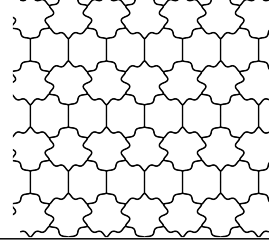
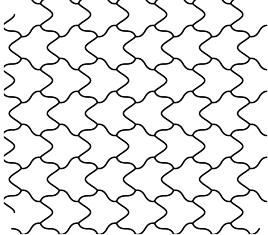
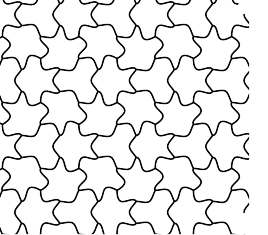
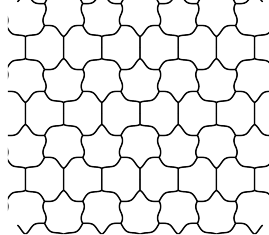
$E_2$				
$T_1$				
$T_2$				
$T_3$				
$T_4$				

Table 4: Post-bifurcated patterns predicted for the equibiaxial loading of the regular hexagonal honeycomb.

Some preliminary observations are possible when studying results presented in Table 4. As expected, the pattern predicted for irreducible representation  $A_1$  is undeformed. Indeed, the symmetry group

of that pattern is the same as the one of the undeformed hexagon and it has already been assessed that irreducible representation  $A_1$  is associated with a symmetry-preserving limit point and not a bifurcation point. However, it can also be observed that irreducible representation  $B_1$  associated with symmetry class  $D_3^s \times (Z_2 \times Z_2)$  seems to produce the same undeformed pattern that the one of irreducible representation  $A_1$ . This is confusing because this symmetry group corresponds to the one of an upright equilateral triangle ( $\blacktriangle$ ) repeated twice along both lattice vectors and a deformation pattern could be expected to appear for this group. This post-bifurcation pattern actually corresponds to the axial displacement of the central node of each beam along the beam direction as presented in Figure 6. It cannot be observed on the nodeless representation proposed in Table 4.

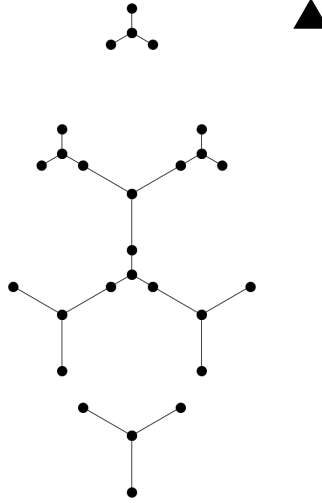


Figure 6: Visualization of post-bifurcated pattern with symmetry group  $D_3^s \times (Z_2 \times Z_2)$ . Dots correspond to finite element nodes.

Furthermore, a thorough observation of Table 4 allows us to confirm that some predicted post-bifurcation patterns are the same as patterns already reported in the literature but obtained through non-linear numerical simulations or experiments. The three post-bifurcated patterns (alternating band Mode I, butterfly Mode II and flower Mode III) corresponding to the equibiaxial loading first symmetry-breaking bifurcation point reported in [13, 14, 15] and obtained by various numerical methods in these articles, are retrieved for the irreducible representation  $T_2$  using the new proposed method. Additionally, the groups  $D_3^h \times (Z_2 \times Z_2)$ , belonging to irreducible representation  $B_2$ , and  $C_6 \times (Z_2 \times Z_2)$ , belonging to irreducible representation  $A_2$ , both produce post-bifurcated patterns qualitatively similar to those found by [6]. Finally, the three modes presented in [15] Fig. 22 corresponding to the deformation patterns after the fifth bifurcation point along the principal path are retrieved by the new proposed method and all three belong to the last irreducible representation  $T_4$ . On this note, this computation invalidates the analysis proposed in [15] to see these modes as higher versions of the alternating band Mode I, butterfly Mode II and flower Mode III. Indeed these modes belong to a different irreducible representation and to different groups. A side-by-side comparison of

the modes obtained in the literature and the ones predicted by the present method is proposed in Figure 7. Note that the modes predicted by the new method may be plotted with a larger amplification factor resulting in more deformed patterns than the ones proposed in the literature. Nevertheless, the qualitative agreement is satisfying.

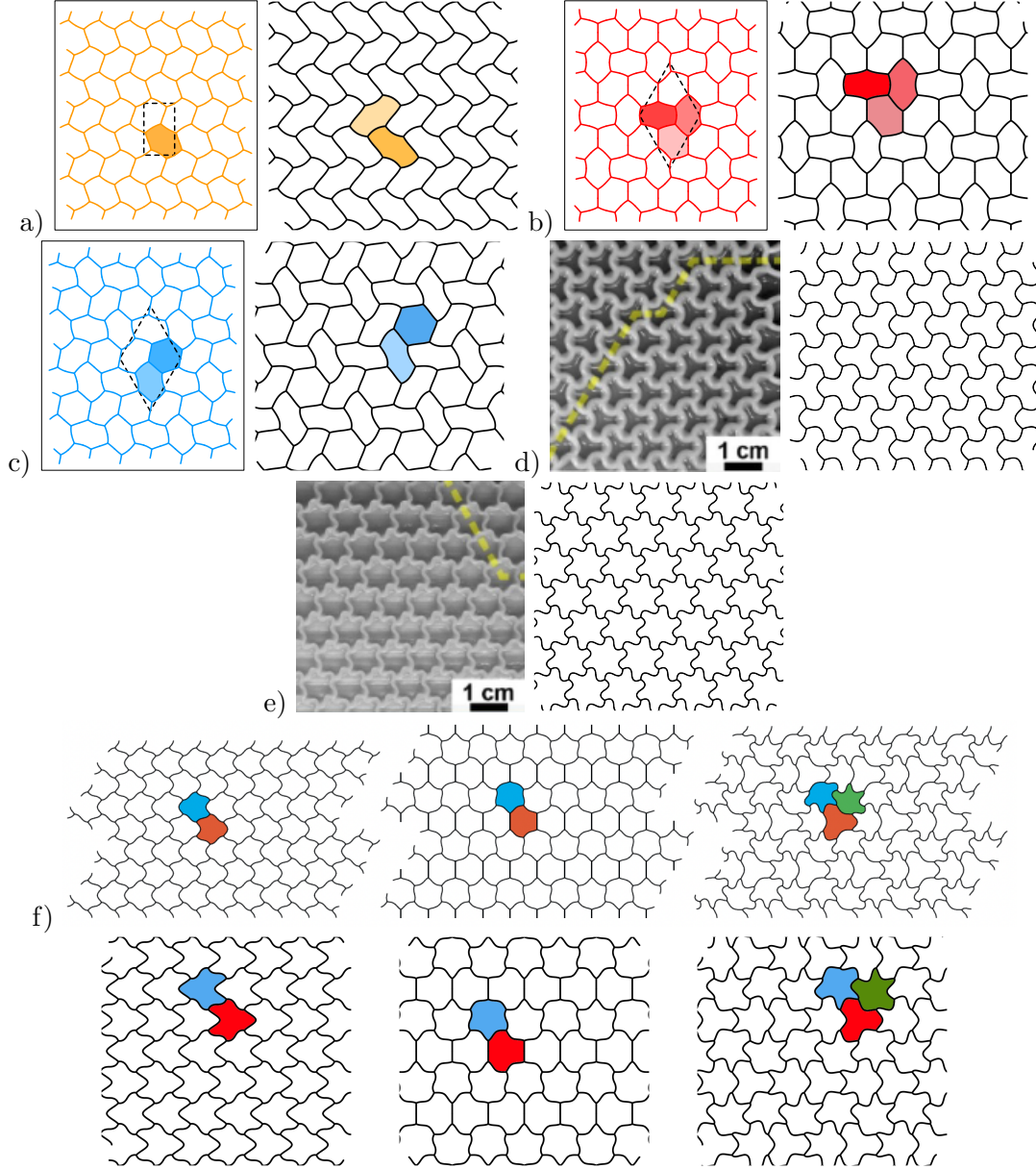


Figure 7: Side by side comparison of modes presented in the literature (left-hand side) and modes predicted by the present method (right-hand side). a) alternating band mode I from [15], b) butterfly mode II from [15], c) flower mode III from [15] d) triangle mode from [6] e) chiral mode from [6] f) three unnamed modes top from higher bifurcation point in [15] and bottom predicted by the new method for irrep  $T_4$ .

The yellow dotted lines in the experimental images taken from [6] visible on Figure 7 d) and e) represent phase shifts where the deformed mode shifts from one group to another one of the same class. Recall that groups belonging to the same class correspond to rotated or mirrored versions of the same deformation pattern. This is visible on the experimental image where the mode on the left of the yellow dotted line in Figure 7 d) corresponds to the mode predicted by the new method and the one on the right of the yellow dotted line is the same pattern but rotated by  $\frac{2\pi}{3}$ . The same happens on Figure 7 e) where the two groups from the same class are mirror images of each other due to the fact that these groups are chiral. These phase shifts cannot be predicted by the present method.

Finally, thanks to the eigenvalue analysis of the stiffness matrix, higher-order post-bifurcation patterns are accessible by plotting eigenvectors corresponding to non-minimal eigenvalues. The modes corresponding to the second lowest eigenvalue for irreducible representation  $T_2$  are plotted in Figure 8. These modes are in perfect accordance with the modes presented in [15] Fig.22 for the fourth bifurcation point along the principal path. As a consequence, these modes are indeed higher-order versions of the alternating band Mode I, butterfly Mode II and flower Mode III. This hypothesis raised from [15] is thus confirmed for the modes of the fourth bifurcation point but not those stemming from the fifth bifurcation point. This additional information results from the use of the present method.

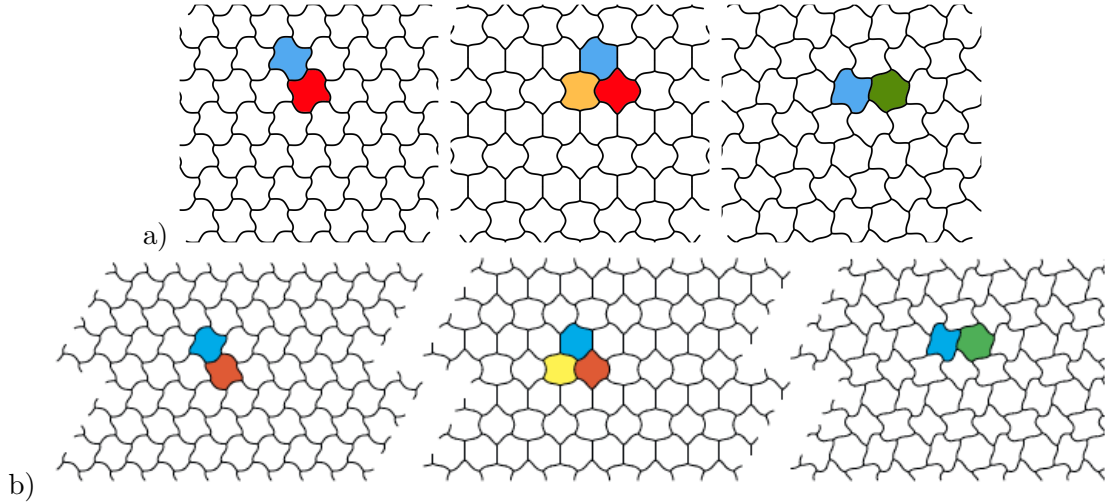


Figure 8: Comparison of a) the post-bifurcated patterns corresponding to the second lowest eigenvalue of the stiffness matrix for the three symmetry groups of the irreducible representation  $T_2$  and b) the computed post-bifurcated deformation modes belonging to the fourth bifurcation point along the principal path from [15]

As a conclusion for this analysis of equibiaxial loading conditions , for the minimum eigenvalue a total of seventeen possible post-bifurcation patterns are predicted by the method. Eight post-bifurcated patterns, already reported in the literature and obtained through non-linear finite element simulations or experimental realisations, have been retrieved by the new proposed method thus serving

as a validation for our method. Nine additional new patterns are predicted. The presented method also gives access to higher energy patterns that may correspond to higher-order bifurcation points happening further away along the principal path. Indeed, three of such patterns, all associated with the same irreducible representation, have been reported to happen further along the principal path in non-linear numerical simulations in the literature.

#### 4.4 Uniaxial and Biaxial loadings

The attention is now focused on uniaxial or biaxial loadings. For both these cases, The symmetry group of the boundary conditions is  $D_2$ , the symmetry group of the rectangle. This group is composed of four elements: two reflections and two rotations which leave the boundary conditions invariant (Figure 9). The symmetry group to study is again the intersection between the symmetry group of the geometry and that of the loading. In this case it corresponds to  $D_6 \times (Z_2 \times Z_2) \cap D_2 \equiv D_2 \times (Z_2 \times Z_2)$ . The reader's attention is drawn to the fact that, if the mirror axes of symmetry for the loading are not aligned with those of the initial geometry, the resulting intersection symmetry group might be lower. This case will not be considered here.

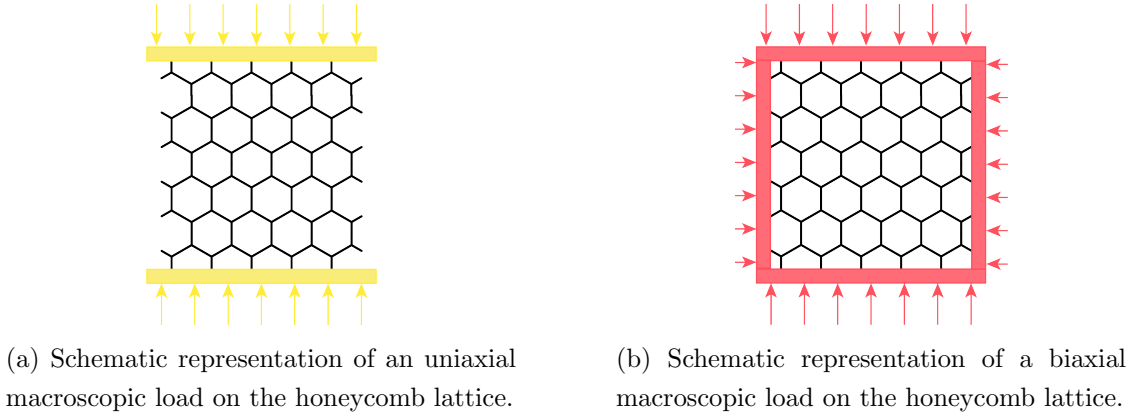


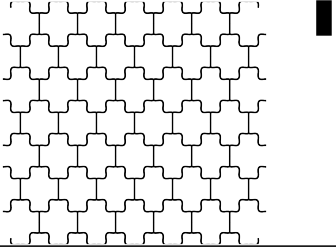
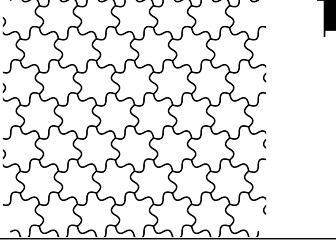
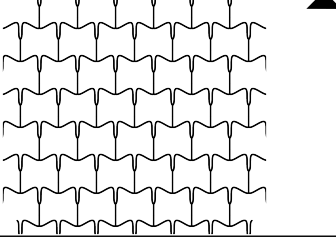
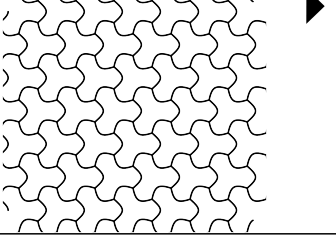
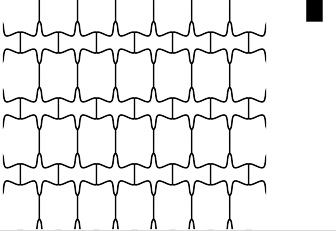


Figure 9:  $D_2$  (rectangular ) loading conditions.

According to the GAP software, the symmetry group  $D_2 \times (Z_2 \times Z_2)$  possesses 10 irreducible representations: eight one-dimensional, named  $A_i$  or  $B_i$  for  $i \in 1..4$ , and two two-dimensional named  $E_1$  and  $E_2$ . For this group, the new method predicts only 12 possible post-bifurcated symmetry classes. For the first 8 irreducible representations, only one post-bifurcated subgroup class may exist, whereas two classes compete for the 9th and 10th irreducible representations. These classes along with the associated predicted post-bifurcated patterns are presented in Table 5. Most of these symmetry classes have the symmetry of a rectangle except for group  $C_2$  which is a chiral group i.e. it does not have any mirror symmetry but only the half-turn rotational symmetry. It could be represented by the symmetry group of a rectangular helix  as presented in Table 2.

Irreducible Representation	Symmetry class	Post-bifurcated patterns
$A_1$	$D_2 \ltimes (Z_2 \times Z_2)$	
$A_2$	$C_2 \ltimes (Z_2 \times Z_2)$	
$A_3$	$D_1^s \ltimes (Z_2 \times Z_2)$	
$A_4$	$D_1^h \ltimes (Z_2 \times Z_2)$	
$B_1$	$D_2 \ltimes Z_2$	

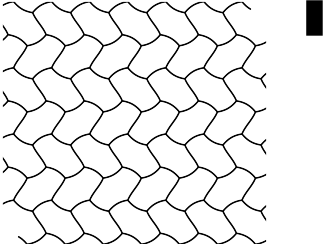
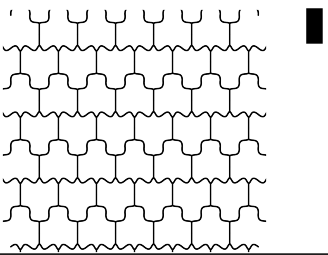
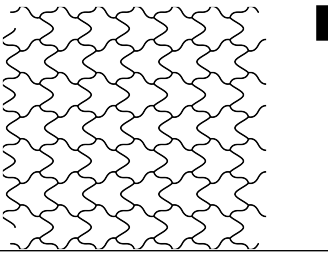
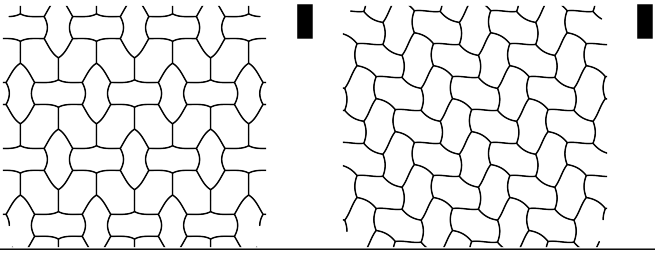
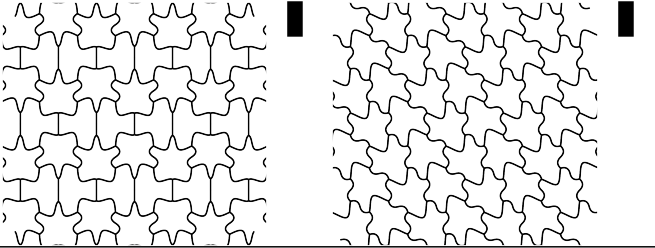
$B_2$	$D_2^g \ltimes Z_2$	
$B_3$	$D_2^{g^2} \ltimes Z_2$	
$B_4$	$D_2^{g^3} \ltimes Z_2$	
$E_1$	$D_2 \mid C_2 \ltimes Z_2$	
$E_2$	$D_2^{g^2} \mid D_2^{g^2}$	

Table 5: Symmetry classes and associated Post-bifurcated patterns predicted for the uniaxial or biaxial loading of the regular hexagonal honeycomb.

From observing results presented in Table 5, the first observation is that the deformed mode predicted for the trivial irreducible representation  $A_1$  is not a bifurcation mode, it simply corresponds to the deformed configuration of a regular hexagonal honeycomb loaded along its mirror symmetry axes.



A more interesting phenomenon is observed for irreducible representations  $A_2$  and  $A_4$ . Indeed for these irreducible representations, the predicted pattern belongs to a symmetry group that has more symmetries than the predicted symmetry group. See for instance the post-bifurcated deformed pattern arising from irreducible representation  $A_2$  that appears to be  $C_6 \ltimes (Z_2 \times Z_2)$  which is a supergroup (i.e. it has more symmetry elements) of its predicted symmetry group  $C_2 \ltimes (Z_2 \times Z_2)$ . Indeed,  $C_6$  group encompasses symmetry elements corresponding to rotations by  $\frac{2k\pi}{6}$ ,  $k \in [1, \dots, 6]$  where  $C_2$  group only has the rotation by  $\frac{2\pi}{2} = \pi$ . This interesting phenomenon is explained by the fact that the energy minimisation argument cannot prevent the solution from having more symmetry than its symmetry class.

For validation purposes, the results are now compared to previously obtained patterns from the literature. The alternating band mode I has been obtained both experimentally and numerically in previous literature studies [1, 16] using uniaxial compression loading. It appears when the structure is loaded parallel to the struts and arises from a one-dimensional irreducible representation. Using the new proposed method, this mode appears as the post-bifurcated pattern related to irreducible representation  $B_2$  which is indeed one-dimensional. This mode seems to be also identified in the two-dimensional irreducible representation  $E_1$  but with a different orientation. It is important to note that, even if alternating band modes from irreducible representations  $B_2$  and  $E_1$  seem identical they are in fact not since tilted ovals of the  $E_1$  mode are different in sizes from one orientation to another. For this irreducible representation two possible post-bifurcated patterns are identified which correspond quantitatively to the two modes presented in [16] since they share the same generators. The  $D_2$  butterfly mode has also been observed experimentally by [1] using biaxial loading. Figure 10 presents side-by-side comparisons of the experimental observations by [1] and the predicted modes using the new method. The qualitative comparison shows a good agreement. Finally, the new proposed method predicts 8 new possible bifurcation patterns for uniaxial or biaxial loadings.

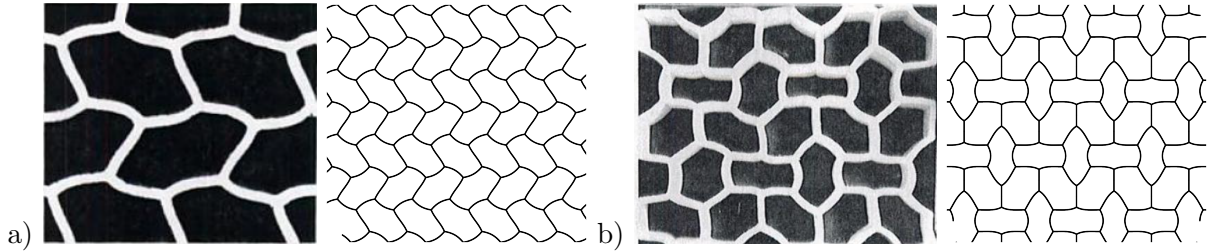


Figure 10: Side by side comparison of modes presented in the literature (left-hand side) and modes predicted by the present method (right-hand side). a) alternating band mode I obtained experimentally under uniaxial compression from [1], b) butterfly mode II obtained experimentally under biaxial compression from [1]

## 5 Conclusion

In this work, a new method for predicting the post-bifurcated patterns of architected material is presented. This method is based on group-theoretic tools. It predicts a larger number of possible post-bifurcated patterns than other proposed methods in the literature without performing any nonlinear computation thus making it suitable for integration into design processes. Additionally, the method is carried out entirely independently of any imperfection parameter or any asymptotic method. Obtaining the post-bifurcated patterns is easily achieved by a simple eigenvalue analysis of the stiffness matrix once the degrees of freedom have been reduced.

The method still admits some limitations that are listed now. The periodicity of the post-bifurcated patterns has to be postulated at the beginning of the study when the unit cell is chosen. Authors believe that this limitation could be lifted using some additional group-theoretic tools to represent the unit-cell periodicity. However, in the current state, authors advise taking advantage of the speed of the method along with its possible parallelisation to assess various unit-cell sizes iteratively. Another limitation of this method is that it is not exhaustive since it relies on the application of the Equivariant Branching Lemma which is only a sufficient condition for the existence of an emerging bifurcated path with a given symmetry group. To the authors' knowledge, this limitation cannot be lifted yet since the most generalised version of the Equivariant Branching Lemma has already been used in the present method. A last limitation is the fact that the present method cannot discriminate between the various post-bifurcated patterns appearing for multiple-dimensional irreducible representations nor can predict which invariant subspace will become unstable first along the principal path. Authors are currently working on energy arguments to uniquely determine the effective post-bifurcated pattern arising at the multiple bifurcation points corresponding to these multiple-dimensional irreducible representations. The first limitation is easily lifted by any linear or non-linear bifurcation analysis and will require precisely defining the loading. This can be done in an additional step of the process after using this method. This process has been already tested and will be presented in a coming companion article.

Furthermore, the authors are emphasizing that, even if the method has been presented in the application using finite beam elements, it is not limited to these elements and can be implemented using any other type of finite element **keeping in mind that the energy minimisation argument is mostly justified when linear buckling analysis is applicable**. Similarly, the considered application is on 2D architected materials but the method is applicable without modification to any 3D architected material. **Finally, the presented post-bifurcated patterns only correspond to the periodic part of the real pattern and are predicted close to the bifurcation point. Their evolution along the bifurcated path is not predicted and, if localization phenomenon or phase shifts appears this cannot be captured by this method.**

The method has been implemented in Python and is coupled with the Group, Algorithms, Program-

ming software for handling the group-theoretic computations. With its current state of implementation, the method only requires from the user the basic knowledge of group theory that consists in being able to identify the symmetry group of the working unit-cell provided at the first step of the method. The method then automatically takes care of the remaining group theoretical computations and analysis and provides the possible post-buckling patterns as an output. The Python program is available on the Zenodo platform [32].

A validation of the method by application to the regular hexagonal honeycomb has been presented. Observed patterns from experimental and numerical studies of the literature are retrieved along with nine new post-bifurcated patterns for this type of honeycomb. The method can adequately take into account the loading by considering the intersection of its symmetry group with the one of the initial geometry at the beginning of the process. Authors believe that the predicted post-bifurcated buckling modes of a given architected material can be used as an input to homogenisation methods in order to predict the behaviour of a full structure composed of such material. A first step in this direction has been attempted in [33] where it has been found that a micromorphic model should be preferred over strain-gradient models in order to take into account periodic bifurcation in the equivalent homogenised model. Using the three modes of equibiaxial loading, a numerical micromorphic homogenisation process has been implemented and successfully captured the appropriate buckling modes [34].

Finally, in view of designing architected material in a *Material-by-design* approach, the proposed method introduces the design parameters at two separate stages as presented in Figure 1 b). As a consequence, a specific design loop can assess material parameters at an intermediate stage of the process thus making the new method perfectly suited for design applications. The loading being an additional design parameter of its own to induce a given post-bifurcated pattern in an architected material, its precise definition is not needed in the current method and can be added as a separate third stage in order to determine the first bifurcation point along the principal path.

## Declaration of competing interests

The authors declare that they have no known competing financial interests or personal relationships that could have appeared to influence the work reported in this paper.

## 6 Acknowledgments

This work was supported by Agence Nationale de la Recherche, France through the ANR MAX-OASIS project (Grant No. ANR-19-CE08- 0005). Authors wish to thank Pr. Ryan S. Elliott and Pr. Nick Triantafyllidis for their insightful remarks on this work.

## References

- [1] M. Ashby, “Designing architected materials,” *Scripta Materialia*, vol. 68, pp. 4–7, Jan. 2013.
- [2] N. Fleck, V. Deshpande, and M. Ashby, “Micro-architected materials: Past, present and future,” *Proceedings of The Royal Society A: Mathematical, Physical and Engineering Sciences*, vol. 466, pp. 2495–2516, July 2010.
- [3] S. D. Papka and S. Kyriakides, “In-plane compressive response and crushing of honeycomb,” *Journal of the Mechanics and Physics of Solids*, vol. 42, pp. 1499–1532, Oct. 1994.
- [4] S. D. Papka and S. Kyriakides, “Biaxial crushing of honeycombs: —Part 1: Experiments,” *International Journal of Solids and Structures*, vol. 36, pp. 4367–4396, Oct. 1999.
- [5] S. D. Papka and S. Kyriakides, “In-plane biaxial crushing of honeycombs—: Part II: Analysis,” *International Journal of Solids and Structures*, vol. 36, pp. 4397–4423, Oct. 1999.
- [6] S. H. Kang, S. Shan, W. L. Noorduin, M. Khan, J. Aizenberg, and K. Bertoldi, “Buckling-Induced Reversible Symmetry Breaking and Amplification of Chirality Using Supported Cellular Structures,” *Advanced Materials*, vol. 25, no. 24, pp. 3380–3385, 2013.
- [7] C. Gao, V. Slesarenko, M. C. Boyce, S. Rudykh, and Y. Li, “Instability-Induced Pattern Transformation in Soft Metamaterial with Hexagonal Networks for Tunable Wave Propagation,” *Scientific Reports*, vol. 8, p. 11834, Aug. 2018. Number: 1 Publisher: Nature Publishing Group.
- [8] N. Triantafyllidis and M. W. Schraad, “Onset of failure in aluminum honeycombs under general in-plane loading,” *Journal of the Mechanics and Physics of Solids*, vol. 46, pp. 1089–1124, June 1998.
- [9] D. Okumura, N. Ohno, and H. Noguchi, “Post-buckling analysis of elastic honeycombs subject to in-plane biaxial compression,” *International Journal of Solids and Structures*, vol. 39, pp. 3487–3503, June 2002.
- [10] R. Azulay, C. Combescure, and J. Dirrenberger, “Instability-induced pattern generation in architected materials — A review of methods,” *Int. J. Solids Struct.*, vol. 274, no. May 2022, p. 112240, 2023.
- [11] N. Ohno, D. Okumura, and H. Noguchi, “Microscopic symmetric bifurcation condition of cellular solids based on a homogenization theory of finite deformation,” *Journal of the Mechanics and Physics of Solids*, vol. 50, pp. 1125–1153, May 2002.
- [12] M. Golubitsky, I. Stewart, and d. schaeffer, *Singularities and Groups in Bifurcation Theory: Volume II*. Applied Mathematical Sciences, Singularities and Groups in Bifurcation Theory, New York: Springer-Verlag, 1988.

- [13] I. Saiki, K. Ikeda, and K. Murota, “Flower patterns appearing on a honeycomb structure and their bifurcation mechanism,” *International Journal of Bifurcation and Chaos*, vol. 15, pp. 497–515, Feb. 2005. Publisher: World Scientific Publishing Co.
- [14] K. Ikeda and K. Murota, *Imperfect Bifurcation in Structures and Materials: Engineering Use of Group-Theoretic Bifurcation Theory*. Springer Science & Business Media, Sept. 2010.
- [15] C. Combescure, P. Henry, and R. S. Elliott, “Post-bifurcation and stability of a finitely strained hexagonal honeycomb subjected to equi-biaxial in-plane loading,” *International Journal of Solids and Structures*, vol. 88-89, pp. 296–318, June 2016.
- [16] C. Combescure, R. S. Elliott, and N. Triantafyllidis, “Deformation patterns and their stability in finitely strained circular cell honeycombs,” *Journal of the Mechanics and Physics of Solids*, vol. 142, p. 103976, Sept. 2020.
- [17] A. Vanderbauwhede, “Symmetry and bifurcation near families of solutions,” *Journal of Differential Equations*, vol. 36, pp. 173–187, May 1980.
- [18] T. J. Healey, “A group-theoretic approach to computational bifurcation problems with symmetry,” *Computer Methods in Applied Mechanics and Engineering*, vol. 67, pp. 257–295, Apr. 1988.
- [19] C. J. Combescure, T. J. Healey, and J. Treacy, “A Group-Theoretic Approach to the Bifurcation Analysis of Spatial Cosserat-Rod Frameworks with Symmetry,” *J. Nonlinear Sci.*, vol. 33, no. 2, 2023.
- [20] A. Zingoni, “On the symmetries and vibration modes of layered space grids,” *Eng. Struct.*, vol. 27, no. 4, pp. 629–638, 2005.
- [21] A. Zingoni, “Group-theoretic insights on the vibration of symmetric structures in engineering,” *Philos. Trans. R. Soc. A Math. Phys. Eng. Sci.*, vol. 372, no. 2008, 2014.
- [22] I. Kiyohiro, M. Kazuo, and F. Hiroshi, “Bifurcation hierarchy of symmetric structures,” *Int. J. Solids Struct.*, vol. 27, no. 12, pp. 1551–1573, 1991.
- [23] Y. Chen, R. Xu, C. Lu, K. Liu, J. Feng, and P. Sareh, “Multi-stability of the hexagonal origami hyper based on group theory and symmetry breaking,” *Int. J. Mech. Sci.*, vol. 247, no. November 2022, p. 108196, 2023.
- [24] K. Gatermann, “Computation of bifurcation graphs,” *Exploiting Symmetry in Applied and Numerical Analysis, AMS Lectures in Applied Mathematics*, vol. 29, pp. 187–201, 1993.
- [25] A. P. Cracknell, “Irreducible representations of point groups and space groups - the last 50 years and the next 10 years,” pp. 227–241, 1980.

- [26] R. McWeeny, *Symmetry: An introduction to group theory and its applications*. Courier Corporation, 2002.
- [27] E. Ihrig and M. Golubitsky, “Pattern selection with  $O(3)$  symmetry,” *Physica D: Nonlinear Phenomena*, vol. 13, pp. 1–33, Aug. 1984.
- [28] K. Gatermann, *Computer algebra methods for equivariant dynamical systems*. Springer, 2007.
- [29] Y. Kosmann-Schartzbach, *Groups and Symmetries, from finite groups to Lie groups*. 2010.
- [30] G. Zhang, N. Feng, and K. Khandelwal, “A computational framework for homogenization and multiscale stability analyses of nonlinear periodic materials,” *International Journal for Numerical Methods in Engineering*, vol. 122, no. 22, pp. 6527–6575, 2021.
- [31] The GAP Group, *GAP – Groups, Algorithms, and Programming, Version 4.12.2*, 2022.
- [32] R. Azulay, C. Combescure, and J. Dirrenberger, “3PAM : Prediction of Post-bifurcated Patterns of Architected Materials,” Nov. 2023.
- [33] C. Combescure, “Selecting Generalized Continuum Theories for Nonlinear Periodic Solids Based on the Instabilities of the Underlying Microstructure,” *J Elast*, 2022.
- [34] O. Rokoš, M. M. Ameen, R. H. Peerlings, and M. G. Geers, “Extended micromorphic computational homogenization for mechanical metamaterials exhibiting multiple geometric pattern transformations,” *Extrem. Mech. Lett.*, vol. 37, p. 100708, 2020.